

A Proposal for the DarkLight Experiment at the Jefferson Laboratory Free Electron Laser

J. Bernauer, W. Bertozzi, R. Cowan, K. Dow, C. Epstein, P. Fisher *, S. Gilad, A.
Kelleher, Y. Kahn, R. Milner, R. Russell, J. Thaler, C. Tschalaer, A. Winnebeck

*Laboratory for Nuclear Science, Massachusetts
Institute of Technology, Cambridge, MA 02139, USA*

S. Benson, J. Boyce, D. Douglas, R. Ent, P. Evtushenko, H.
C. Fenker, J. Gubeli, F. Hannon, J. Huang, K. Jordan, G.
Neil, T. Powers, D. Sexton, M. Shinn, C. Tennant, S. Zhang
Jefferson Lab, 12000 Jefferson Avenue, Newport News, VA 23606

M. Freytsis

Physics Dept. U.C. Berkeley, Berkeley, CA

R. Fiorito, P. O'Shea

*Institute for Research in Electronics and Applied
Physics University of Maryland, College Park, MD*

R. Alarcon, R. Dipert

Physics Department, Arizona State University, Tempe, AZ

G. Ovanessian

Los Alamos National Laboratory, Los Alamos NM

-Ellie Long

M. Kohl

*Physics Dept., Hampton University, Hampton, VA 23668 and Jefferson Lab,
12000 Jefferson Avenue, Newport News, VA 23606*

T. Horn

Physics Dept., Catholic University of America, Washington, DC 20064

* Corresponding author (fisherp@mit.edu)

I realize I'm new to
the experiment, but I
was wondering
would it would take
for me to be listed
on this proposal?

Isn't adding "of the photon" redundant since α_{EM} is already mentioned?

(Dated: May 1, 2012)

Is it important to note the Wattage since this is a fixed target experiment? Wouldn't putting the required current be more useful?

New theories of dark matter predict A' gauge bosons in the mass range of 0.01–10 GeV that couple to charged fermions with a strength of $\alpha' \alpha_{EM} = 10^{-4}$ of the photon or less. We propose to design, construct and operate an experiment called DarkLight (Detecting A Resonance Kinematically with eElectrons Incident on a Gaseous Hydrogen Target) to use the 1 MW 100 MeV electron beam at the Jefferson Lab Free Electron Laser incident on a 10^{19}cm^2 thick target to study the process $e^- + p \rightarrow e^- + p + e^- + e^+$. A dark force particle would show up as a narrow resonance in the radiated $e^+ A' e^-$ system. Our experiment would explore the A' mass region 10-100 MeV and couplings as low as $\alpha' \sim 10^{-9}$ with 1/ab of data, which would require 60 days of data taking (assuming 100% efficiency) at the Jefferson Lab Free Electron Laser. We also plan for 30 days of running (assuming 100% efficiency) for beam studies, calibration and commissioning.

Is 100% normal for FEL experiments?

I thought A' would couple DM, not exist in leui of it?

I. INTRODUCTION

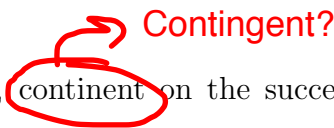
Dark matter comprises 23% of the energy of the universe, and in the past ten years detection of dark matter and elucidation of its nature has moved to the forefront of experimental particle physics. Until recently, axions and weakly interacting massive particles (WIMPS) were the favored candidates and the focus of experimental investigation. Recent results, however, from both underground and cosmic ray experiments suggest that dark matter may be explained by a new theory that predicts vector or scalar bosons in the 10 MeV–10 GeV mass range that couple to electrons and positrons. Current experimental bounds limit the coupling to less than 10^{-2} – 10^{-3} of the QED coupling, depending on the boson mass. This motivates us to consider experiments able to probe this new theory using a 1 MW, 100 MeV electron beam at the Jefferson Laboratory Free Electron Laser (FEL).

Same as above

The DarkLight experiment is designed to search for a narrow resonance in the e^+e^- spectrum of elastic electron-proton scattering below pion threshold (i.e. at 100 MeV incident electron energy). Such a resonance will rest on the QED radiative tail. The final state proton recoils with low kinetic energy and DarkLight is designed to detect all final state particles using a large acceptance toroidal magnetic spectrometer. Vertex detectors for both recoil

proton and final-state leptons are planned as well as large drift chambers in each sector of the magnetic toroid. The windowless gas target with multi-stage differential pumping system is embedded in the magnetic solenoid.

In December 2009, we submitted a letter of intent to carry out a new experimental search using the JLab FEL. The LOI was favorably reviewed by PAC35. We submitted a proposal to PAC37, requesting conditional approval to carry out beam tests and background measurements at the FEL to ensure we can achieve the beam control and background conditions necessary to carry out the experiment. Conditional approval was granted and we have a beam test scheduled for July 2012.

We now seek full approval for DarkLight,  contingent on the success of the beam test. If DarkLight receives approval, this will allow the DarkLight collaboration to begin working with the DOE to secure funding for the operation of the FEL and construction of the detector. This proposal outlines our physics case (Section II), the FEL and detector designs (Sections III and IV), expected performance (Section VI) and required resources and schedule (Section VII).

II. PHYSICS MOTIVATION

Recent interest in new light bosons has been sparked by their possible connection to dark matter physics. Here, we summarize the dark matter motivation for new A' bosons, and list some existing experimental constraints and search strategies.

A. Dark Matter and Dark Forces

By now, the gravitational evidence for dark matter is overwhelming [? ? ? ?]. While the precise nature and origin of dark matter is unknown, thermal freezeout of a weakly interacting massive particle (WIMP) is a successful paradigm that arises in many theories beyond the standard model. In the WIMP paradigm, dark matter is a TeV-scale particle that interacts with standard model particles via electroweak interactions. There is a wide range of searches that are sensitive to WIMPs, including direct detection in nuclear recoil experiments, direct production in collider experiments, and indirect detection in cosmic ray experiments.

In the past two years, however, a new paradigm for dark matter has emerged where dark matter is still a TeV-scale particle, but interacts dominantly through a “dark force” [? ? ? ?]. The carrier for this (short-range) force is a new GeV-scale gauge boson DarkLight particle, which we refer to as A' . To confirm this new paradigm, ~~one~~ would like to gain direct evidence for this A' boson.

These dark force models are motivated by three astrophysical anomalies that hint at excess electron/positron production in the Milky Way: the WMAP Haze [? ?], the PAMELA, FERMI, and H.E.S.S. e^+/e^- excesses [? ? ? ?], and the INTEGRAL 511 keV excess [? ?]. Such dark force models may also play a role in explaining the DAMA annual modulation signal [?]. Intriguingly, these anomalies can be explained in terms of dark matter annihilation, decay, and/or up-scattering in the Milky Way halo, though not with a standard WIMP. Rather, the peculiar features of these anomalies hint that dark matter is interacting with a light A' boson and that A' bosons are being produced in these dark matter interactions. To explain the anomalies while evading other astrophysical bounds, the A' boson must dominantly decay to electrons, muons, pions and/or taus, with little hadronic activity [? ? ?]. In addition, the most recent e^+e^- data gives a Standard Model prediction for $(g-2)_\mu$ which lies 3.6σ away from the measurement [?]. Corrections from a dark force carrier in the 10–100 MeV range could explain this difference.

There are a variety of different dark force scenarios, but the most popular models invoke a new vector boson that kinetically mixes with the standard model photon [? ?]:

$$\mathcal{L} = \epsilon F'_{\mu\nu} F_{\text{EM}}^{\mu\nu}. \quad (1)$$

Isn't A' a gauge boson?

Through this “photonic portal”, the A' boson inherits electromagnetic couplings, albeit with a reduced coupling strength

$$\alpha' = \epsilon^2 \alpha_{\text{EM}}, \quad (2)$$

where $\alpha_{\text{EM}} \sim 1/137$. The coupling α' and the mass $m_{A'}$ are both free parameters in these models. While other dark force models are equally plausible, we focus on the photonic portal case for concreteness, since it is the one most studied in the literature.

B. Searching for the Dark Force

Spurred by this new dark force paradigm, there has been much recent interest on how to find the light A' boson. There is a huge range of $\{\alpha', m_{A'}\}$ values that are consistent with

existing astrophysical measurements, so multiple experiments will be necessary to probe the full parameter space. To date, a number of possible avenues for discovery have been explored, including:

- Production in lepton colliders through $e^+e^- \rightarrow \gamma + X$ [? ? ? ? ? ? ? ?]. When A' decays promptly to $\mu^+\mu^-$, existing B -factory data already places a constraint.
- Production in fixed-target experiments. Previous searches for light axions are also sensitive to A' bosons if A' is sufficiently long-lived [? ?]. There are ongoing effort to do data mining on prior experiments, and Refs. [? ? ?] include a number of new fixed-target proposals. Of particular relevance for Jefferson Lab, the APEX experiment has completed a trial run in Hall A, and the HPS experiment is proposed for Hall B.
- Rare meson decays [? ? ? ?]. Any meson decay that yields a photon could have a suppressed branching fraction to a dark photon. In particular, a reanalysis of KTeV data [?] would be sensitive to $\pi^0 \rightarrow \gamma + X$ with $X \rightarrow e^+e^-$.
- Production in fixed-target experiments with a positron beam [?].

Is X supposed to be A' or DM? Or is it just whatever decay fills in the blank?

However, the muon anomalous magnetic moment results pick out the region $m_{A'} = 10\text{-}100$ MeV [? ?], so DarkLight focusses on this region.

The goal of the present proposal is to study couplings in the range $10^{-9} < \alpha' < 10^{-6}$, and masses in the range $10 \text{ MeV} < m_{A'} < 100 \text{ MeV}$. In this parameter range, the A' boson dominantly decays promptly as $A' \rightarrow e^+e^-$ with $c\tau > 10^{-2}$ cm. This parameter space is illustrated in Fig. 1, with the most important constraints indicated. We believe we can reach couplings in the range $\alpha' = 10^{-9} - 10^{-7}$ over the mass range 10–90 MeV with a 60 days (assuming 100% efficiency) of running at the JLab FEL.

1. Other physics topics

A search for invisible modes in $e^- + p \rightarrow e^- + p$: In addition to the recent interest in $A' \rightarrow e^+e^-$ [1], there is ~~additional~~ motivation for light A' bosons that dominantly decay ~~invisibly~~ through invisible channels. The INTEGRAL 511 keV excess [?] could be interpreted as coming from sub-10 MeV dark matter in the galactic center annihilating through an off-shell A' to e^+e^- pairs [?

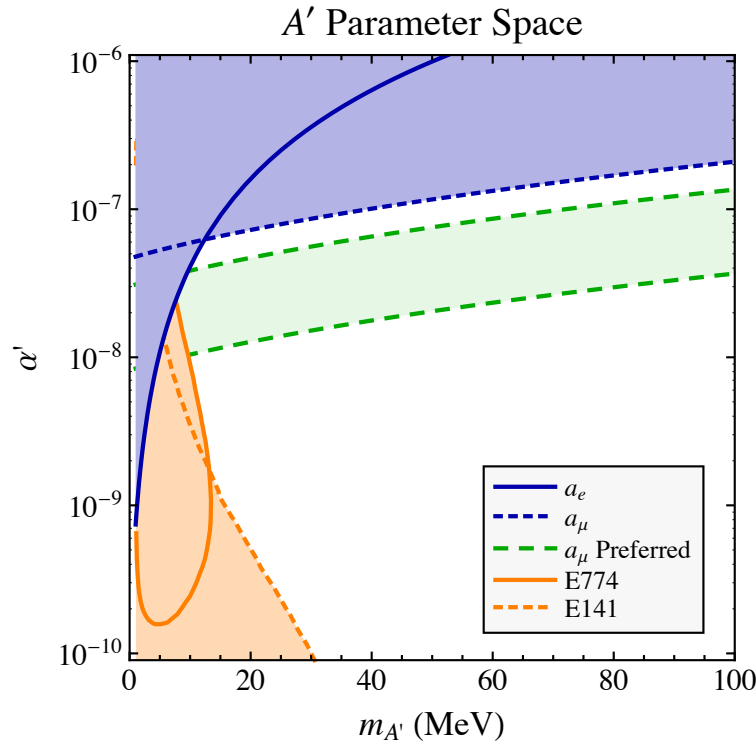


FIG. 1: The A' boson parameter space considered in the proposed search. The blue shaded regions correspond to bounds on the anomalous magnetic moment of the electron (a_e) and muon (a_μ) [? ?]. The A' boson can actually reconcile the 3.6σ discrepancy with the measured value of a_μ in the “ a_μ Preferred” region.. The orange shaded regions correspond to bound from previous beam dump experiments, E774 at Fermilab [?] and E141 at SLAC [?], where the A' boson is sufficiently long-lived to yield a displaced vertex.

???. This A' has both a coupling to e^+e^- pairs as well as to light dark matter particles χ , and in the preferred region of parameter space, the dominant decay is $A' \rightarrow \chi\chi$. One can therefore search for an invisibly decaying A' boson by looking for the process $ep \rightarrow ep + A'$ with $A' \rightarrow \text{inv.}$

There was in fact a proposal to search for such an invisibly decaying A' boson using an energy recovery linac in Ref. [?], but that proposal did not have full kinematic reconstruction, and was unable to control radiative QED backgrounds. With the DarkLight experiment, we will have the ability to fully reconstruct the $ep \rightarrow ep + \text{inv.}$ process, and partially veto photons from the processes $ep \rightarrow ep + \gamma$ and $ep \rightarrow ep + \gamma\gamma$ which can fake an invisible signal.

We are working on developing the experimental concept and so do not yet have a clear idea of the sensitivity.

How much do we know? Wouldn't it be better to put that in?

Should this whole section be an appendix for a parasitic experiment? It feels out of place here and might work better as a bonus later on?

Measurement of the proton charge radius using $e - p$ scattering: The electromagnetic form factors of the proton at low Q^2 have long been one of the interesting measurements in the standard model. Such measurements have gained renewed interest with the recent measurement of the muonic Lamb shift [?], which suggest a different value of proton charge radius than previous extractions using ep scattering data [? ? ?] and determinations from spectroscopy of electronic hydrogen [? ? ?]. Since the proton charge radius $\langle r_p^2 \rangle$ is defined in terms of the slope of the electric form factor $G_p^E(Q^2)$ as

$$\langle r_p^2 \rangle = -6 \left. \frac{dG_p^E(Q^2)}{dQ^2} \right|_{Q^2=0}$$

precise and accurate measurements of $G_p^E(Q^2)$ can be used to extract the proton charge radius and compare to the recent measurements.

With an electron beam energy of 100 MeV and an electron acceptance between 25° and 165° , DarkLight is sensitive to Q^2 values in ep elastic scattering between 0.0019 (GeV/c)^2 , a factor of 2 smaller value than [?], and 0.033 (GeV/c)^2 , with even lower values accessible with a lower beam energy and extended forward acceptance.

Using a model for G_p^M , the proton charge radius can be extracted from a measurement at one energy alone, since the cross section at forward angles and low Q^2 is dominated by the electric form factor.

A variation of the beam energy will allow us to separate the form factors using the Rosenbluth technique model independently. The comparatively small Q^2 values even at backward angles give us the opportunity to determine both G_p^E and G_p^M with good precision in this low Q^2 regime, where only few reliable data points exist. Such a separation would also yield precise charge and magnetization radii. While it is hard to determine the absolute cross section with uncertainties small enough to add a meaningful data set to the world data, it should be possible to fix the global normalization with an extrapolation of the cross section or of the form factors to $Q^2 = 0$, where their values are known, a method already used in [?]. In the upcoming month, we plan to work out the feasibility of this method.

C. Invisible final states

Discontinuity in how decays are presented. It would look better if we were consistent throughout

DarkLight is designed to search for an A' boson through $ep \rightarrow epA' \rightarrow epe^+e^-$. We can also use the experiment to search for invisibly decaying A' : $ep \rightarrow epA'$ where we only

observe the electron and proton. Possible backgrounds are $ep \rightarrow ep\gamma$, $ep \rightarrow ep\gamma\gamma$, and pileup where we mis-reconstruct the outgoing 4-vectors from two or more different events. We will argue that assuming *no* photon detection, the *only* irreducible background is $ep \rightarrow ep\gamma\gamma$, and hence our reach is dramatically improved by adding photon detection. The kinematics for the remaining kind of events, including pileup, are different enough from the signal that they can in principle be eliminated.

We make the following assumptions about the DarkLight setup: electrons are detected from $25^\circ - 165^\circ$, protons are detected from $5^\circ - 89^\circ$ (N.B. the upper limit should be changed to 63° based on our conversation yesterday. will fix that by early next week), $(87\%) \times 2\pi$ azimuthal coverage, photon detection (if available) only for $E_\gamma > 1\text{MeV}$.

Notation: we consider the processes $e^-p \rightarrow e^-px$, where $x = \gamma, \gamma\gamma, A'$, etc. We denote the incoming four-vectors as $p_{e^-} \equiv p_1, p_p \equiv p_2$, and the outgoing four-vectors as $p'_{e^-} \equiv p_3, p'_p \equiv p_4$. For most of the analysis, we assume *zero* photon detection efficiency (i.e. all photons are invisible); we make some comments at the end about how the reach improves with photon detection. We first consider possible backgrounds where only one event is seen during the timing window, and then consider the effects of pileup.

Most of these can be eliminated just by considering whether the “missing invariant mass” is nonzero or not. Assuming full kinematic reconstruction, the quantity $p_1 + p_2 - p_3 - p_4$ is strictly zero for an elastic event, or for a single photon event, $ep \rightarrow ep\gamma$. Indeed, with a 1 MeV invariant mass resolution, the number of these events which can fake an invariant mass of 10 MeV is well below the number of signal events given our design luminosity. ~~If the mass range is restricted to $m_{A'} > 10\text{MeV}$, this background can be ignored entirely. if we restrict to searching for $m_{A'} \gtrsim 10\text{MeV}$, we can ignore this background entirely.~~ With

zero photon detection efficiency, the main irreducible background for the invisible search is two-photon bremsstrahlung, $ep \rightarrow ep\gamma\gamma$. The two photons can have a broad invariant mass spectrum, and the cross-section for this QED process is larger than the corresponding signal process $ep \rightarrow epA'$ by a factor of α/α' . Note that even with photon detection, the process $ep \rightarrow ep\gamma\gamma$ where both photons go down the beampipe poses an irreducible background.

D. Negative invariant mass trick

Now consider the case of pileup, where an elastic event $p_1 + p_2 \rightarrow p_3 + p_4$ and any other event $p_1 + p_2 \rightarrow p'_3 + p'_4 + q$ (where q is invisible) occur during the same trigger window.

Why do this? It doesn't save much typing and requires frequent reference back to this section

Why the quotes?

Maybe move this up here?

Suppose the electron from the second event is mis-reconstructed as belonging to the elastic event:

$$p_1 + p_2 \rightarrow p'_3 + p_4 \quad (3)$$

Then, since $p_1 + p_2 = p_3 + p_4$ from four-momentum conservation in the elastic event, we have the ~~missing invariant mass~~

$$\begin{aligned} m^2 &= (p_1 + p_2 - p'_3 - p_4)^2 \\ &= (p_3 + p_4 - p'_3 - p_4)^2 \\ &= (p_3 - p'_3)^2 \\ &= 2m_e^2 - 2E_3E'_3 + 2\sqrt{(E_3^2 - m_e^2)(E'^2_3 - m_e^2)} \cos \theta_{33'} \\ &\leq 2m_e^2 - 2E_3E'_3 + 2\sqrt{(E_3^2 - m_e^2)(E'^2_3 - m_e^2)} \end{aligned}$$

It turns out that this expression is strictly nonpositive, and is zero only when $E = E'$. Identical arguments hold for the other mis-reconstructed event, with the electron mass and energies replaced by the corresponding quantities for the proton, but the functional form of m^2 is unchanged.

For exactly two events in the timing window, we have the following possibilities:

- Background: $ep/ep, ep/ep\gamma, ep/ep\gamma\gamma, ep\gamma/ep\gamma$
- Signal: $ep/epA', ep\gamma/epA'$

Even more notation types?

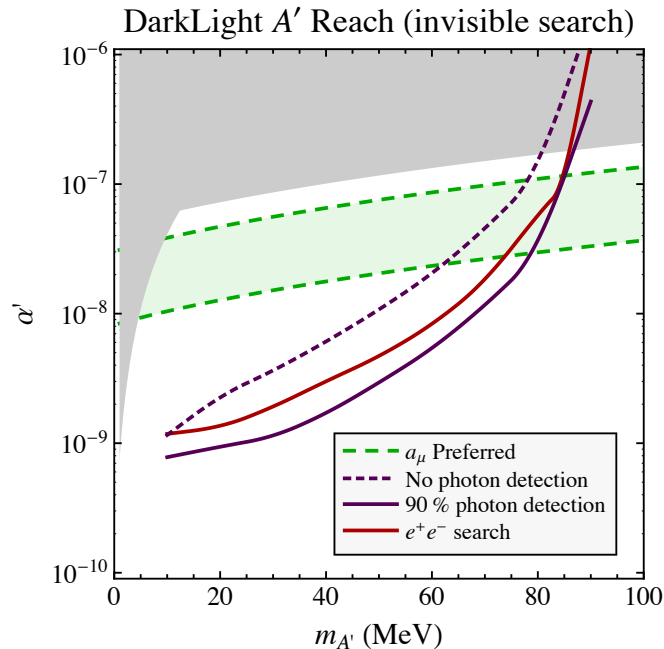
Assuming we see all four charged tracks, we now pair both electrons with both protons to form four invariant masses: $m^2_{11}, m^2_{12}, m^2_{21},$ and m^2_{22} , where m^2_{ij} means the invariant mass from pairing electron i with proton j . A signal event is defined by having one of the masses, say m^2_{11} , equal to zero (from the elastic or single-photon event), and the other “diagonal” mass positive and equal to $m^2_{22} = (m_{A'})^2$. We first veto any event where there is no invariant mass greater than 10 MeV: by the negative invariant mass trick this eliminates the first two background processes, which contain elastic events with only zero or negative invariant masses. We then veto any remaining event with $m^2_{11} > (10\text{MeV})^2$ and $m^2_{22} \neq 0$. This gets rid of the $ep\gamma/ep\gamma$ events where one of the pairs fakes a large invariant mass, except in the case where the other pair happens to have exactly zero invariant mass. Finally, we can veto events with precisely three zero invariant masses, which effectively removes the $ep\gamma$

3 0-invariant masses? 3.0 invariant masses? 30 invariant masses? It's not entirely clear

pileup background. This leaves only $ep/ep\gamma\gamma$, which has the same kinematics as ep/epA' ; we thus simply ignore the spurious negative or zero invariant masses, and count the single positive invariant mass, so $ep\gamma\gamma$ contributes as an irreducible background exactly as it did for non-pileup events.

The details of this complicated vetoing procedure are not so important, but the upshot is **pileup of two events can in principle be eliminated as a background for the invisible search**. We leave a careful study of 3-event pileup to future work.

Since ~~we can eliminate~~ **pileup can be eliminated** in principle, we compute our experimental reach using only $ep\gamma\gamma$ as background. If we assume a nonzero photon detection efficiency ϵ , then the cross-section for the background scales as $(1-\epsilon)^2$, since ~~one would have to miss~~ **would have to be missed** both photons in a $\gamma\gamma$ event in order for the background to fake a signal. (Of course, this simple picture is distorted somewhat when one or both photons leave the tracking region from $25^\circ - 165^\circ$.) ~~But~~ Since the statistical fluctuations in the background scale as the square root of the number of background events, the overall reach increases approximately linearly with $1-\epsilon$. In other words, if the probability that we miss a photon decreases by a factor of 2, then our reach improves by approximately a factor of 2 throughout the whole mass range. Taking into account the photon kinematics and requiring a 5σ signal-to-background significance, we find the following reach for the invisible search:



The shaded areas represent excluded regions of parameter space from constraints on the

electron and muon anomalous magnetic moment. The green region represents the discrepancy between experimental and theoretical values for $(g - 2)_\mu$, such that the discovery of an A' with mass and coupling within the band would explain the discrepancy. We see that even with modest (90%) photon detection efficiency, we can probe the vast majority of the preferred region. Indeed, the invisible search reach is stronger than the DarkLight e^+e^- search reach across all of parameter space.

III. THE FREE ELECTRON LASER

As the only currently operating free electron laser (FEL) based on a CW superconducting energy recovering linac (ERL), the Jefferson Laboratory FEL Upgrade remains unique as an FEL driver [? ?]. The present system represents the culmination of years of effort in the areas of SRF technology, ERL operation, lattice design, high power optics and DC photocathode gun technology. The layout of the JLab FEL Facility is shown in Fig. 2. The machine as it stands delivers 7 micron emittance bunches of 135 pC at average currents up to 10 mA (74.85 MHz repetition rate). The present beam energy is 135 MeV although it has operated up to 160 MeV in the past. The system has lased in the 0.364 to 11 micron region and produced up to 14.3 kW of average power at 1.6 microns. At lower powers it can tune rapidly over factors of 8 in wavelength. The stable performance of this machine over many years establishes a solid foundation for future light sources and other applications such as the experiment proposed in this report.

The ERL accelerator is comprised of a 9 MeV injector generating up to 9.3 mA of current (nominally in bunches of up to 135 pC at a maximum rep. rate of 74.85 MHz), a linac consisting of three Jefferson Lab cryomodules generating a total of 80 to 125 MeV of energy gain, and a recirculator. The latter provides beam transport to, and phase space conditioning of, the accelerated electron beam for the FELs and then returns and prepares the drive beam for energy recovery in the linac. The beam is typically accelerated (energy recovered) off crest (off trough) so as to impose a phase energy correlation on the longitudinal phase space used in subsequent transport to longitudinally match the beam to the required phase space at the wiggler (dump). That is to say, the bunch is kept relatively long during acceleration, compressed to high peak current and approximately 100 fs rms pulse lengths just before the wiggler, then temporally expanded before reinsertion into the energy recovery phase of the

Is this relevant to DarkLight?

10 kW IR/UV/THz Free-Electron Laser

This is a really low resolution image -- surely there's a higher rez one?

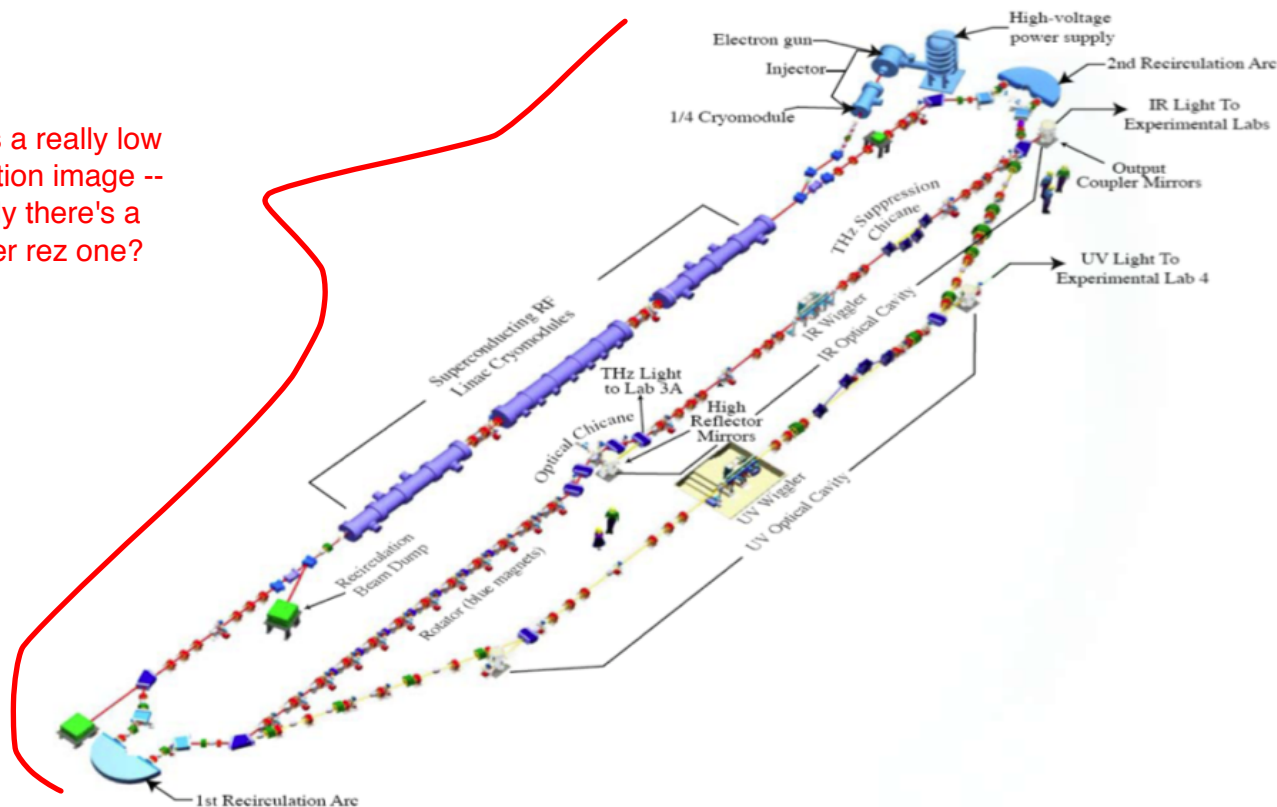


FIG. 2: Schematic of the existing JLab light source facility.

linac. The recirculation transport is, however, operationally flexible and can accommodate configurations providing very small momentum spread to users - though at commensurately longer bunch length.

The electron beam can be sent through the IR wiggler beam path or through the UV wiggler. Switching between the operational modes is accomplished by shorting half the coils of the corner dipoles. The energy recovery transport consists of a second Bates-style end loop followed by a six-quad telescope. The beam is matched to the arc by the second telescope of the FEL insertion; the energy recovery telescope matches beam envelopes from the arc to the linac acceptance. During FEL operation, energy recovery occurs off-trough. The imposed phase-energy correlations are selected to generate energy compression during energy recovery, yielding a long, low momentum spread bunch at the dump. Calculations and measurements show that the emittance growth due to Coherent Synchrotron Radiation (CSR) is not a problem for lower charges but may impact operation at higher charge. As

indicated above, this operating mode can be modified to provide small momentum spread and longer bunches; this will alleviate CSR-driven beam quality degradation.

For the proposed DarkLight experiment, the machine will operate in either a different on-crest acceleration scheme or with a cross-phased tuning, so as to provide smaller momentum spread and longer bunch, instead of the nominal off-crest now used for FEL operation. It is desired that both beam-halo and emittance be eventually measured at the experimental location - the UV wiggler pit. In view, ~~however~~, of up-coming FEL programmatic activities (including removal of the current UV wiggler and installation of a new one, and an IR FEL run for the Navy program), schedule constraints in the near term motivate performing initial halo measurements in the 3F region on the IR line. This choice has the added advantage of performing initial halo studies in the most operationally flexible and heavily instrumented region of the system.

The FEL has gained extensive experience and has in place the necessary beam controls to deal with halo along the beam line. However, it will be necessary to remove the halo-monitor from its legacy position downstream of the second recirculation arc and reinstall it in a cross near 3F06 region on the IR line. In regard to the relevance of halo measurements at the IR beamline as opposed to on the UV beamline, it has been pointed out that although this location is not where the DarkLight experiment is eventually intended to take place, the measurement will provide valuable experience and data needed for a preliminary beam analysis, uncover potential effects that may be seen in the final location, and thus inform the design of the beam line to the DarkLight detector in the UV section of the ERL accelerator.

It is desirable for this experiment to run the accelerator at lower energy (100 MeV), low charge (10-20pC), and high repetition rate (748.5MHz) in order to reduce the emittance of the electron beam. In order to run the machine this way for the DarkLight experiment, certain modifications and additions to the electron photocathode gun drive laser and to the injector tuning are needed, which will be detailed in the following discussion.

A. Roadmap to DarkLight ERL Operation

Present performance of the JLab FEL ERL Driver is largely consistent with DarkLight requirements, save for demonstration of the specific machine setup and adequate halo characterization and management. We propose a three-step route to prepare the ERL for DarkLight

production runs.

The initial step will be a test intended to provide an existence proof of a machine configuration which will allow adequate halo management. In order to complete this activity in a timely manner and at low cost, this test will be performed on the IR side of the system. A halo monitor (currently installed after the second recirculation arc, see section III B) will be modified (as required to allow it to mimic DarkLight aperture constraints), and moved to the FODO array upstream of the final bunch compressor near 3F06 region. This region of the machine is heavily instrumented, provides a large number of focusing and steering controls, and has an installed nonlinear element (an octopole) that has already been used to modify large amplitude components of the beam during beam tuning.

Is it worth defining this the first time it's mentioned?

We have at least two options for the test. The first involves a modification of the 5-quad rotator, removing the center skew quad and retuning the remaining four quads to provide the required Horizontal-Vertical (H-V) phase space interchange (there is a proof-of-principle solution for this tuning that will be tested before any beamline modifications occur). This option is attractive in that it will allow operation of the machine at full current during the halo test. The second alternative is to replace one of the existing beam line viewers in the FODO array with the halo monitor. This will allow testing with tune-up beam and/or at CW currents up to the order of 1 mA, but this option may generate beam envelopes outside of the acceptance of the H-V interchange and may as a consequence preclude operation above the "nominal" beam break up (BBU) threshold. In either case, we will explore halo as a function of single bunch charge, and thus test the option of running very high repeat at low charge (748.5 MHz x 13.5 pC) as a space-charge-induced halo mitigation method.

The second step will be to characterize halo so as to provide the information required to manage it at the location of the DarkLight detector. This will be done using two studies, one presently under way and one proposed. The first study, performed by a collaboration lead by the UMD [?], uses a masking method to capture and characterize halo behavior (see subsection III C). The second study involves large dynamic range (LDR) measurements of beam properties (see subsection III D).

With measurement of emittance at high current and the degree of mismatch of the halo relative to the core beam, we will be positioned to complete an analysis of the beam properties and finalize the beamline design required to inject the beam into the DarkLight detector in the UV ERL wiggler pit. In this final step, we will (given a choice of bunch charge and

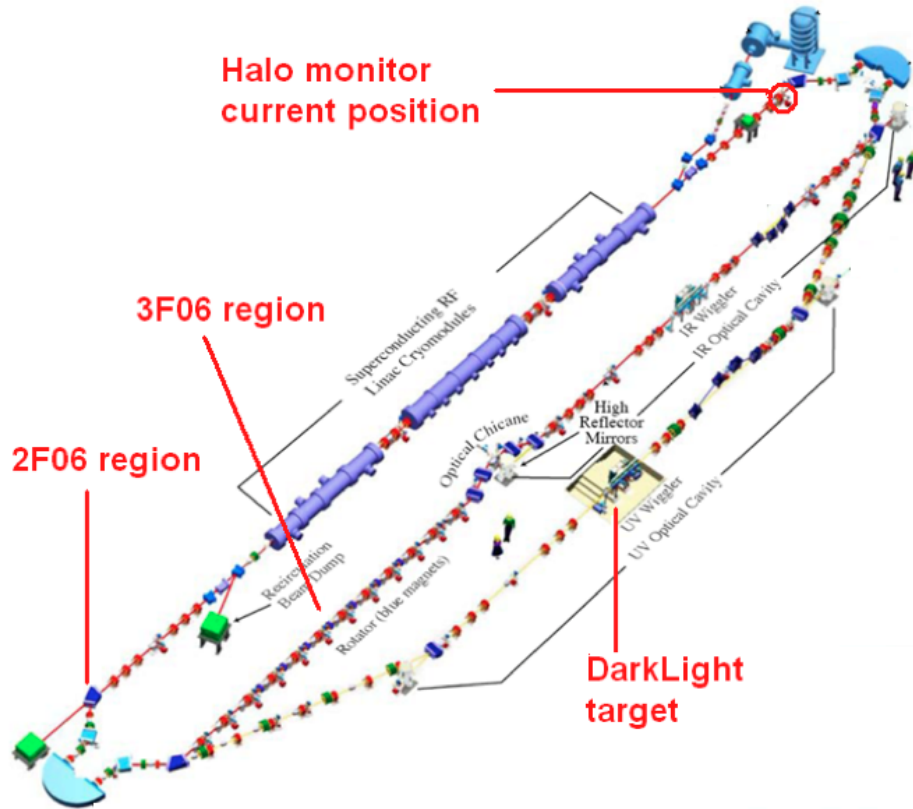


FIG. 3: Illustration of key positions along the JLab ERL accelerator beamline.

injection parameters) complete the longitudinal matching scenario, perform an analysis of beam quality preservation (e.g. with space charge), develop a finalized optics design (including, as needed, H-V interchange and nonlinear envelope management using octopoles), and certify error sensitivities using start-to-end simulation. The finalized solution will be tested on the UV ERL, and halo studies repeated so as to check/optimize procedures for background mitigation once the detector is installed. This activity will include a thorough exploration of the acceptance of the UV recovery transport so as to define the maximum scattering amplitude (and thus the target density and interaction rate) that can be recovered without intolerable beam loss.

The following sections provide detail about specific work activities and hardware needed to implement the aforementioned tests and measurements.

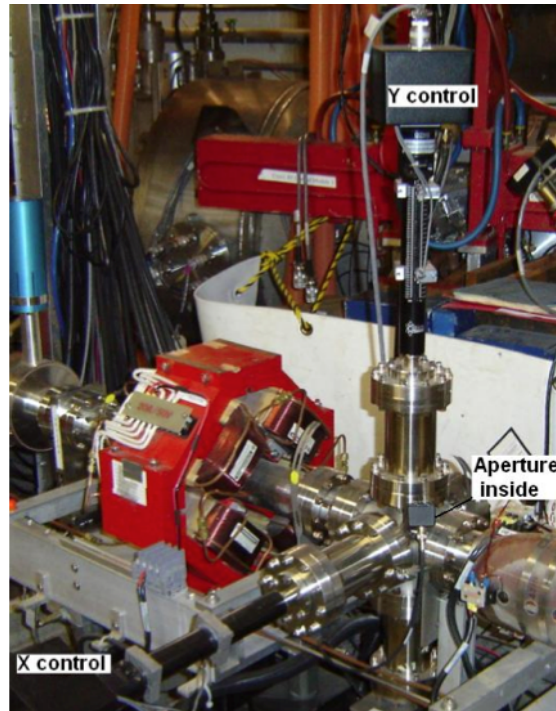


FIG. 4: Existing halo-monitor at 5F10 region.

B. Measurement of Beam-halo with an Existing Halo Monitor

As mentioned earlier, a time and cost effective approach to measure the beam halo would be to remove the existing interceptive halo monitor including the 6-way cross currently installed at the beginning of the linac reinjection region and re-locate it in the middle of the infrared backleg region (near 3F06, see Fig. 3). There is a skew quad currently in that location. The minimum aperture from the current halo monitor is limited to about 5mm, and some reconfiguration (such as off-setting the translation axis and reworking the phosphor forks) will be needed to reduced the aperture size to more closely simulate the smaller (2mm in diameter) aperture of the DarkLight experiment.

Fig. 4 is a picture of the currently existing interceptive beam halo monitoring device located at 5F05 near injector in the FEL vault. The device consists of two 6 stepper motor driven actuators, each fitted with a stepped fork (shown in Fig. 5). A variable step aperture is formed when the two forks move and cross to each other. There is an additional UV LED to illuminate to forks so the camera can be calibrated. When the device is moved the ion pump would remain connected to a replacement Tee, thus minimizing configuration change.

The forks are made of 1/16 Aluminum plate machined in steps of 10mm x 5mm (each

Maybe
add this
to Fig. 4?

What's a Tee?

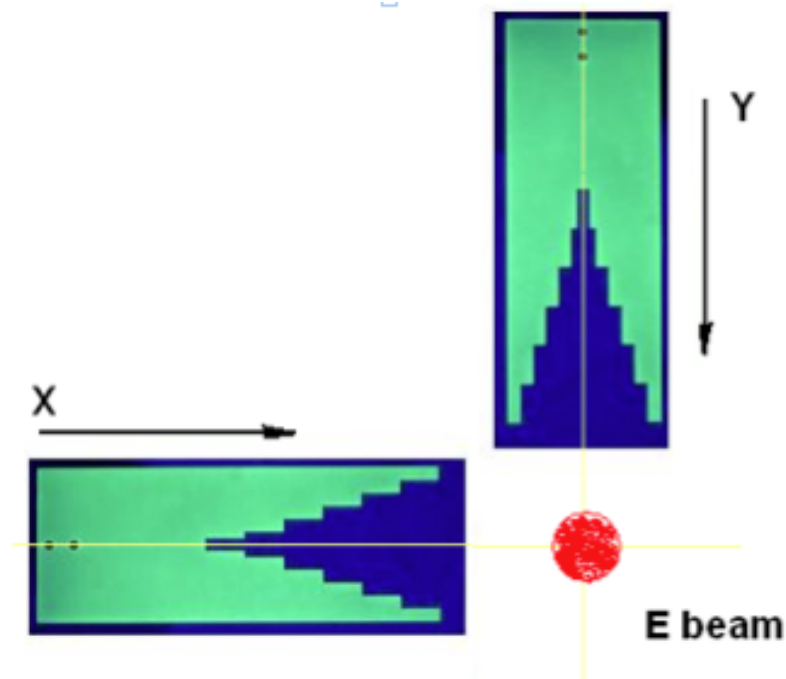


FIG. 5: Halo forks with steps of 5mm x 10mm. Proper off-set on X and Y axis will allow to measure smaller beam size.

side). When inserted all the way they close off the beam path completely. The position is calibrated against the external indicator (steps per mm) and the device is fitted with IN/OUT limit switches. The camera that monitors the device is in-line connected to the tangent point of the last dipole in the second arc. Radiation monitors (BLM PMTs, see more discussion in subsection III F) can also be used to monitor the intercepted beam.

The new location for the interceptive beam Halo monitor would be downstream of the quad girder 3F06. This would require the skew quad be temporarily removed and that an alternative phase-space exchange [?] be implemented. The Halo monitor would be fitted to the existing stand now vacated. The camera view port would again be the tangent point at the last dipole of (now) the first arc. This is used as a HeNe alignment launch point in the current configuration.

C. Non-invasive Beam-halo Measurement

The goal of this activity is to establish a dedicated non-invasive halo monitor for the Dark-Light experiment without any disruption to the beam operation. This will be accomplished

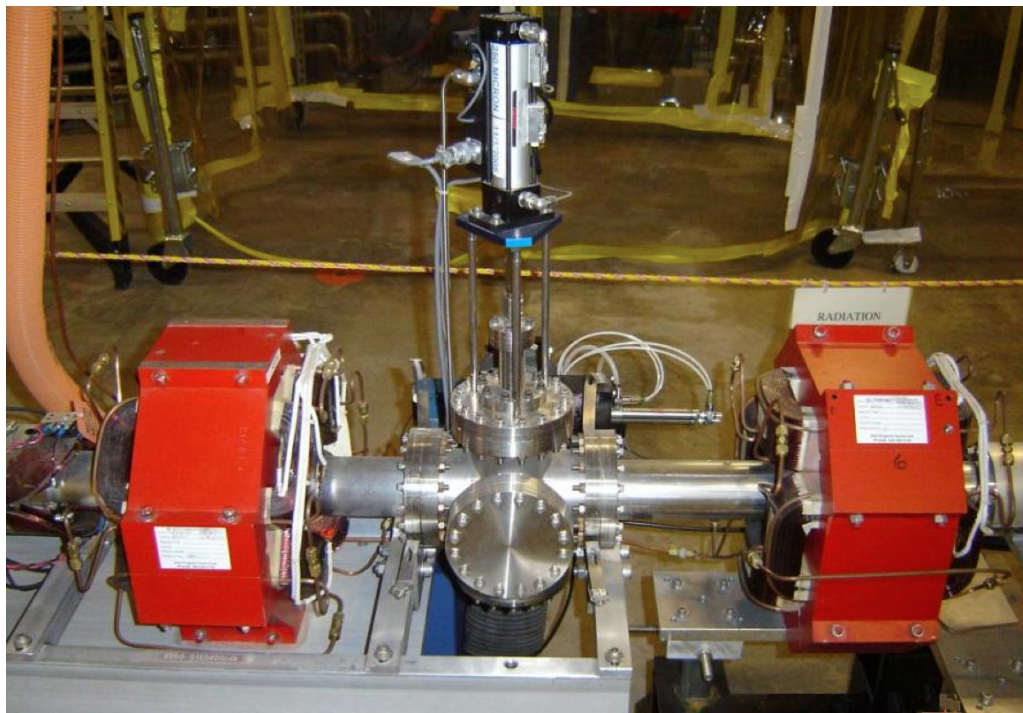


FIG. 6: Picture of quads at 3F06 region on IR beamline. The skew quad is the one on the right.

using Optical Synchrotron Radiation (OSR) which is parasitically produced at chicanes in both the IR and UV lines. We plan to design a flexible optical transport system that can allow observations of the OSR from either the IR or UV lines. Vault ceiling penetrations for either line and are relatively close to ports where the SR can be observed.

The current ceiling penetration for the UV wiggler cables will become available once the UV wiggler is removed, thus providing possibility for the SR light to be transported out of the FEL vault for non-invasive beam-halo measurement. There are a few places where a viewport exists or can be installed to view the SR light. For example, the viewport (clear aperture 35mm in diameter) on the first bending magnet in the chicane up stream of the IR wiggler is immediately available. For the upcoming test in FEL in May, this will be an ideal spot to measure the beam-halo distributions. The electron beam can be imaged through this port the same way as the SR diagnostic system currently setup at 2F06 region. However, a different design of the optical transport is needed in order to do this. A sketch of the relative positions of the viewport and the SR beam path in the FEL vault are shown in Fig. 7. This estimate is subject to revision as details are refined.

A similar optical transport system will have to be built when the DarkLight detector is

?

The wording here is very strange

Do we have higher resolution image for this? It's very difficult to read

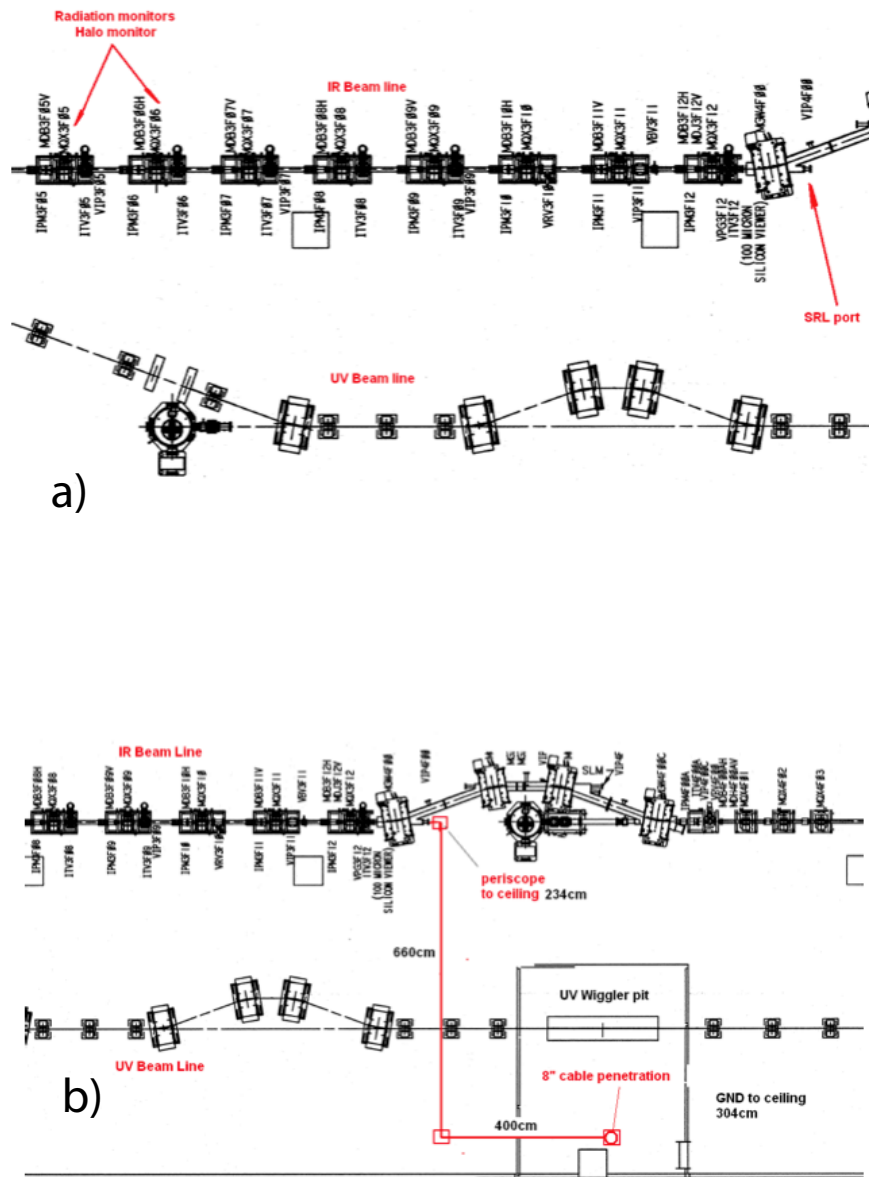


FIG. 7: a) Illustration of intended measurement sites. b) Schematic of beam path for SR optical transport in FEL vault.

installed in the UV wiggler pit. Basically this only requires a modification of the optical system in the FEL vault. The optical components parts on the 2nd floor used for the IR line can be readily adopted to save costs.

D. Large Dynamic Range Beam Emittance Measurement

The beam emittance both upstream and downstream of the UV FEL wiggler location can be measured by quad scans using currently installed viewers. Such measurements were performed recently and the data is being analyzed. It should be pointed out that there are more specific details associated with the beam profile and halo issue for such measurement, which are briefly addressed below.

To study the beam distribution in transverse phase space with large (10^5 - 10^6) dynamic range (LDR), the transverse beam profile needs to be measured over a similar dynamic range and with tune-up beam. In contrast to measurements using CW beam, the electron beam optics can be changed significantly when operating the tune-up beam. This will allow for emittance measurements of the core of the beam as well as the halo of the beam - the part of the distribution with small intensity and potentially large betatron amplitude. When making measurements with tune-up beam, the integrated charge available for the measurement is significantly smaller. Thus, such imaging measurements must employ the process that is most efficient in converting electron beam into light. For LDR measurements with the tune-up beam we will therefore use 100 μm thin optically polished YAG:Ce crystal scintillators. Such beam viewers are already used at the JLab FEL for beam measurements in the injector. Operational experience indicates that with tune-up beam the intensity of the fluorescence will be sufficient for the measurements with the dynamic range of at least 10^5 or even 10^6 . Such measurements will be based on use of two cameras, each with dynamic range of about 10^3 and attenuation effectively different by 10^3 to cover the required range.

E. Upgrade of machine operation mode

Although we will start DarkLight preparation with the currently available 74.85MHz repetition rate and perform important characterizations using bunch charges including 13.5 pC, as mentioned in section III B, it is deemed necessary to reconfigure the machine for operation at higher (748.5 MHz) repetition rate.

Unlike FELs which put stringent requirement on both transverse and longitudinal emittance, the DarkLight experiment only requires high average beam current and small transverse emittance; it places fewer constraints on the longitudinal phase space. This introduces

the possibility of running the accelerator at a much lower bunch charge and at a higher pulse repetition rate. A recent study by F. Hannons shows a much lower emittance may be achieved from the FEL injector with a low bunch charge (approximately 20pC), as shown in Fig. 8. This presents a significant improvement of the e-beam quality and brightness over the present beam which is about 7-8 μm for 135pC bunch charge. It is very straightforward for the accelerator to run a beam at any sub-harmonic frequency of its 1.497GHz driving RF frequency. The question is if we can reconfigure the FEL drive laser to run at a high repetition rate that meets the requirement.

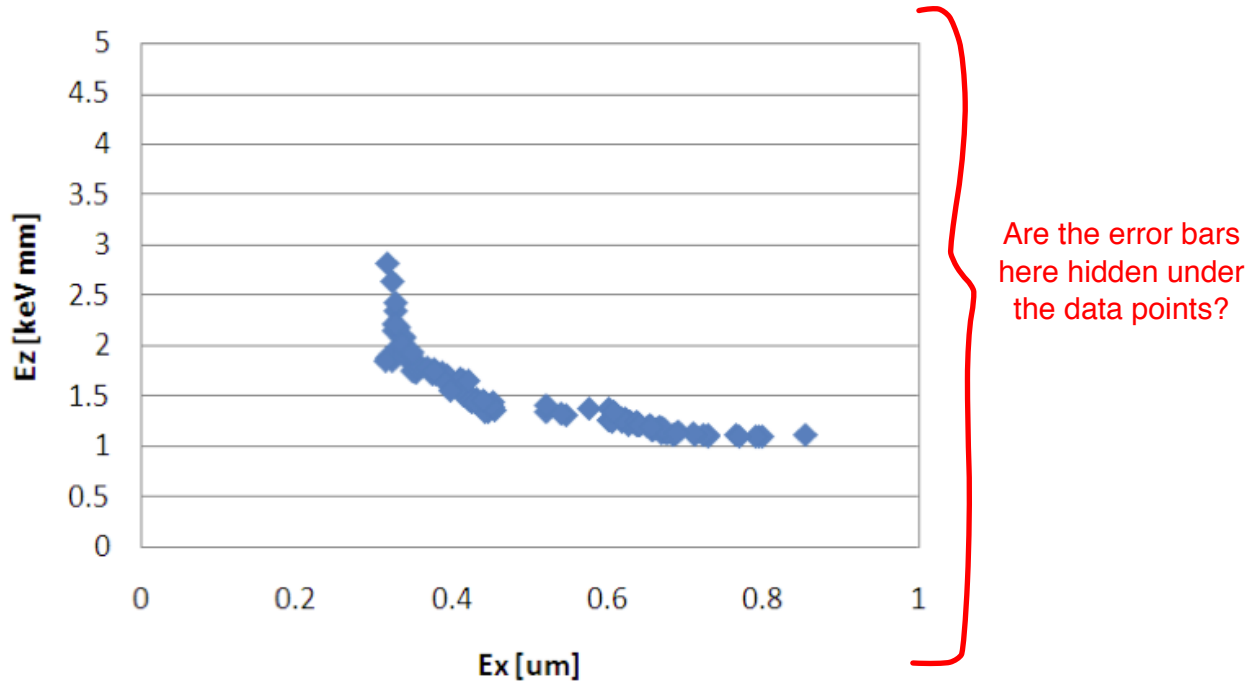


FIG. 8: Result of a beam emittance simulation for 20pC bunch charge from JLab FEL injector.

The FEL photo-cathode drive laser is a new laser system built on the state-of-the-art solid-state laser technology. Ever since it was commissioned, substantial reconfiguration and improvements have been made to keep up with the changing needs for machine operation and various R&D projects. This diode-pumped all-solid-state laser system consists of several sections [?], the oscillator which produces seed pulses, the multi-stage amplifiers, second-harmonic generator (SHG), the beam relay, and pulse control system.

The seed laser is a custom-built diode-pumped Nd:YVO₄, passively mode-locked oscillator with 25 ps pulse width and over 500 mW output power at 1064 nm. This oscillator

can be operated at two distinctively different repetition rates, one is 74.85 MHz (the 20th sub-harmonic of 1.497 GHz) and the other 748.5 MHz (2nd sub-harmonic of 1.497 GHz). The optical configuration has to be changed in order to switch to a different pulse repetition rate. The synchronization to the accelerator is achieved by phase-locking the laser to the RF drive signal. A phase loop actively adjusts the optical cavity length to minimize the pulse timing jitter. The rms timing jitter is usually about 0.5 ps. The amplification system contains four identical diode-pumped amplification modules. The first two amplifiers form a lower power channel (Channel 1) with over 20 W output. When all four amplifiers are running, the maximum power can reach 50 W (output Channel 2). After amplification, the fundamental 1064 nm beam is frequency-doubled to 532 nm in a nonlinear crystal harmonic generator. At 74.85 MHz, the full laser power at 532 nm reaches 8 W from channel 1 and 25 W from channel 2. At 748.5MHz, about 13W was achieved due to lower SHG efficiency.

With the existing FEL photocathode, about 4 W of average laser power at 532nm is needed to generate 10 mA electron beam current. Therefore the available laser power is sufficient if we run drive laser at 748.5 MHz and 10-20 pC bunch charge (the average beam current will be about 10 mA). However, some upgrades over the existing system have to be done before the accelerator machine can operate under such a new beam mode. Specifically, we will need,

1. A new phase control system for 748.5 MHz laser oscillator. The key electronic components inside the phase-loop control chassis have to be replaced to accommodate the higher fundamental frequency. In addition, a new commercial phase-locking unit has to be purchased.
2. Upgrade of the drive laser pulse control system (DLPC) that currently only works at a maximum frequency of 74.85 MHz. The DLPC allows the accelerator to run at various beam-modes, in particular the tune-up mode at low duty-cycle routinely required by the machine optimization.
3. New electro-optic elements and drivers with much faster response.
4. Faster photo-detectors for pulse temporal pulse monitoring.
5. New laser pump diodes to replace the old ones in the laser.

F. Radiation monitors and measurement

To monitor the radiation level or beam loss near the diagnostics and the target, it is necessary to install a modest number of new beam loss probes in the FEL vault. We have had discussions and meetings with the JLab Radiation Control (RadCon) Group in order to make full use of their expertise and understand available resources.

There are basically several options for the detectors to use. The first option is that we can utilize RadCons infrastructure that exists within the FEL and install additional probes and base units. We already have a rapid access monitoring system which is functioning much the way expected for this proposed measurement.

The other option would be to check other vendors for probes that would satisfy the requirements for the measurements. The infrastructure for these units would need to be developed in order to read out these detectors. This is where the information from the suggested calculation and simulations will determine the detector requirements.

It is recommended that proper calculations and/or simulations be performed to help predict the potential radiation based on the present and expected FEL beam parameters such as energy, beam current and potential interaction targets. Also it would be useful to have multiple detectors of both neutron and gamma type at different distances, which may allow measurement of the radiation spectrum. This would be very helpful to the ultimate DarkLight experiment.

G. Radiation monitors and measurement

To evaluate the radiation backgrounds in the FEL vault under typical running conditions, two types of measurements have been made. The first makes use of the existing RadCon Department's radiation monitors. The second uses two NAI/PMT detectors located adjacent to each other and positioned in the vault near the IR beamline, approximately adjacent to the end of the first full-length cryo module FL02.

1. RadCon monitors

Fig. 9 shows the locations of the detectors used in this study. Data from them is available in the FEL stripchart system. A stripchart recording taken during progressive turn-on of

the RF cryo modules is shown in Fig. 10. An increase in the level near the end of FL02 is seen by RM208-2 when FL02 is on. An increase at RM209-2, between FL03 and FL04, is seen when FL03 is on and a further increase when FL04 is on.

The monitor nearest the NAI/PMT detector location, RM208-3, shows a smaller but noticeable increase when FL02 is on, which predominates over contributions from the other cryomodules at this location.

Far too wide -- although I believe LaTeX should fix this?

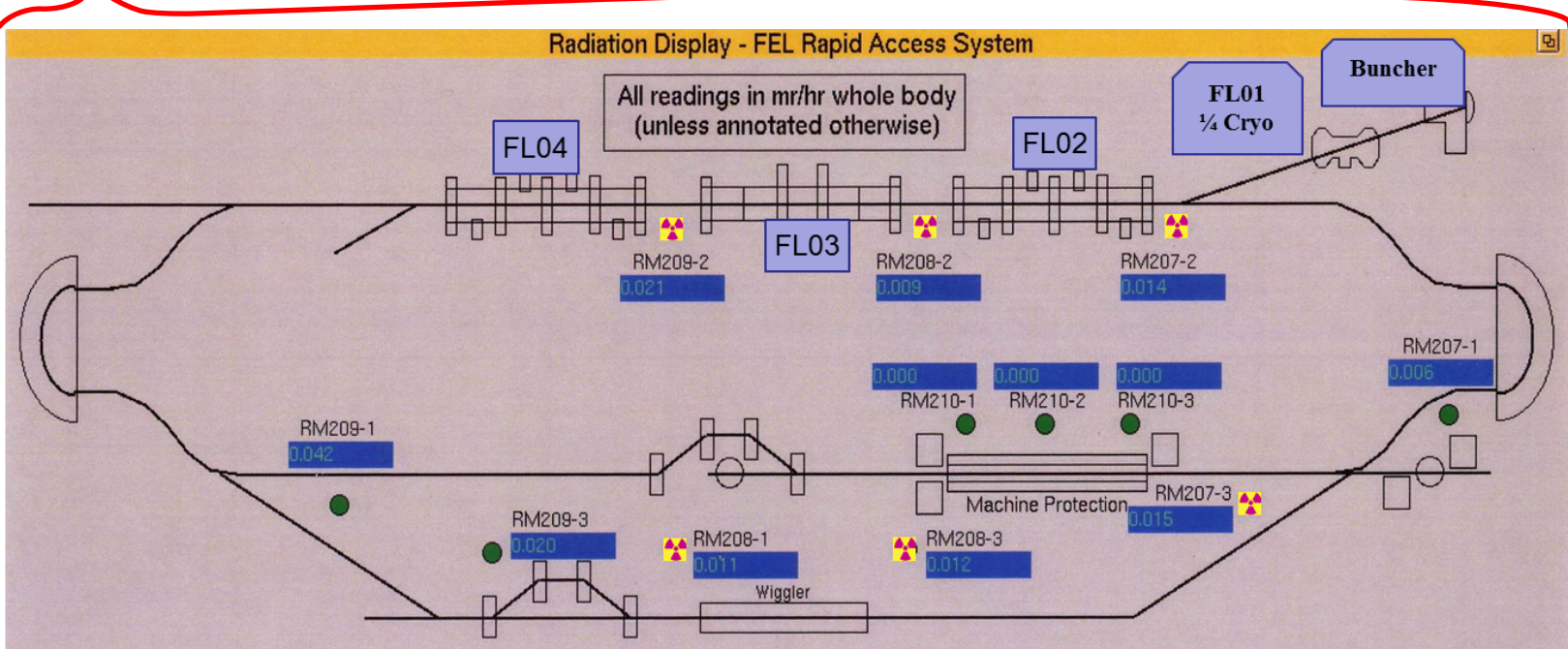


FIG. 9: Location of JLAB RadCon radiation monitors in the FEL vault. Locations are indicated by the trefoil symbols. Of particular interest are monitors RM207-2 (injection point), RM208-2 (between first two full-length cryo modules, FL02 and FL03), RM208-3 (between the IR and UV wigglers, adjacent to the NAI/PMT detectors), and RM209-2 (between the second and third full-length cryo modules, FL03 and FL04).

2. NAI/PMT detector measurements

Two NAI detectors with their associated PMTs, spectroscopy amplifiers, HV supplies, and cabling have been positioned in the FEL vault near the IR line adjacent to the RM208-3 RadCon monitor (See Fig. 11). Readout of each is by two dedicated coaxial cables installed

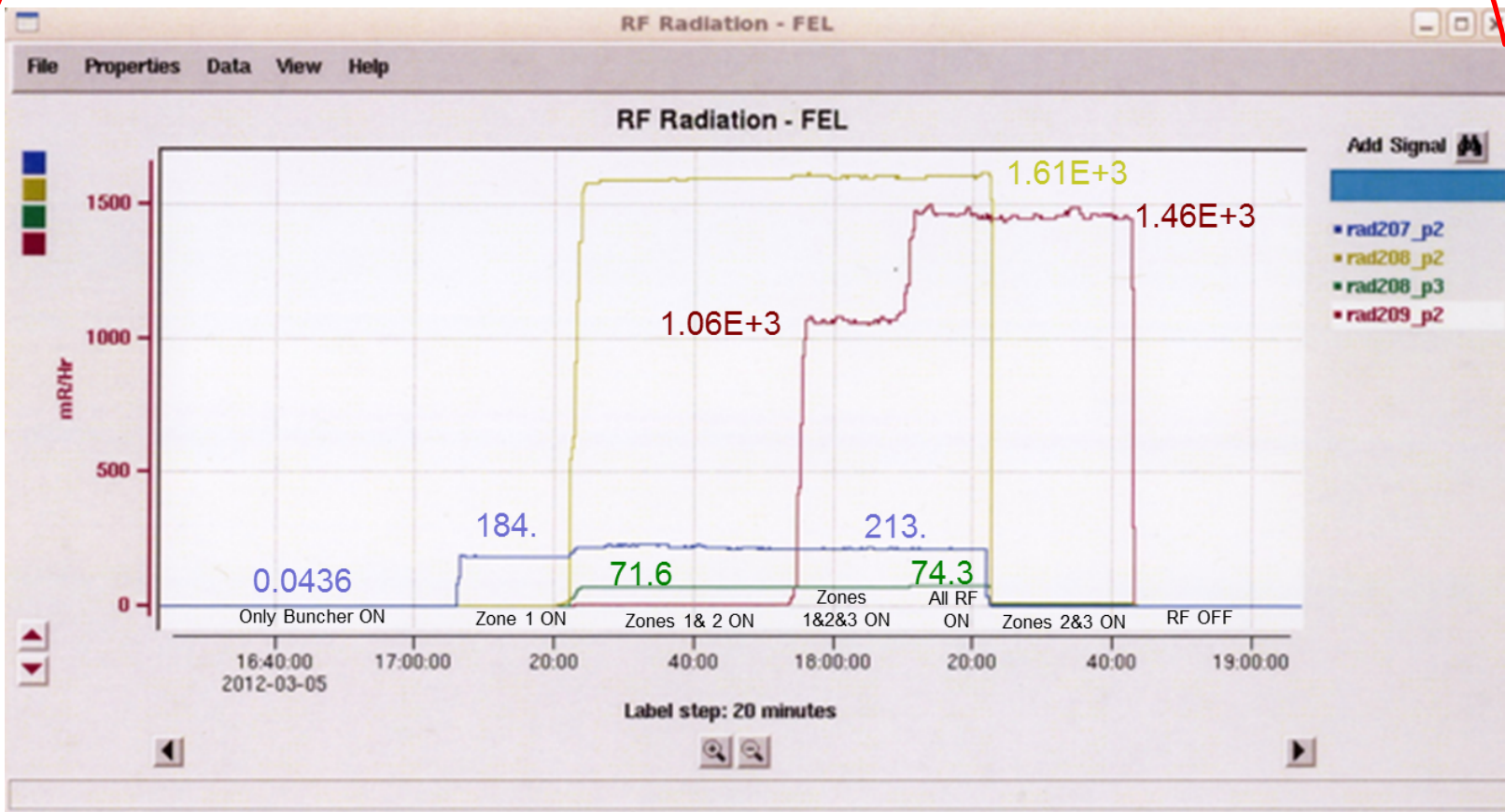


FIG. 10: Radiation levels in the FEL vault measured by selected RadCon monitors. Zones 1–4 refer to cryo modules FL01–FL04. Units are R/hr, whole-body dose.

between the vault and Lab 1 upstairs. Each detector is read out by an MCA and computer in Lab 1. The detectors are at beam height from the floor and housed in lead brick enclosures, with a minimum thickness of 2 inches. (See Fig. 12.)

Sentence needs rewording

Three shielding configurations were studied. The first was the base configuration with 2 inches of Pb surrounding each NAI/PMT on all sides, top, and bottom. A small gap between bricks was left open on the rear for cable access. The second configuration an additional two inches of Pb on the front, top, and sides around the NAI crystal, and the third another additional two inches of Pb. (See Fig. 14.)

The detector setups were calibrated using ^{241}Am and ^{60}Co to cover an energy range from a few tens of keV up to about 2 MeV. Additional cross-checks were performed, ~~including~~ which included checking for noise sources. A run was made with the PMT HV turned off, while the RF was

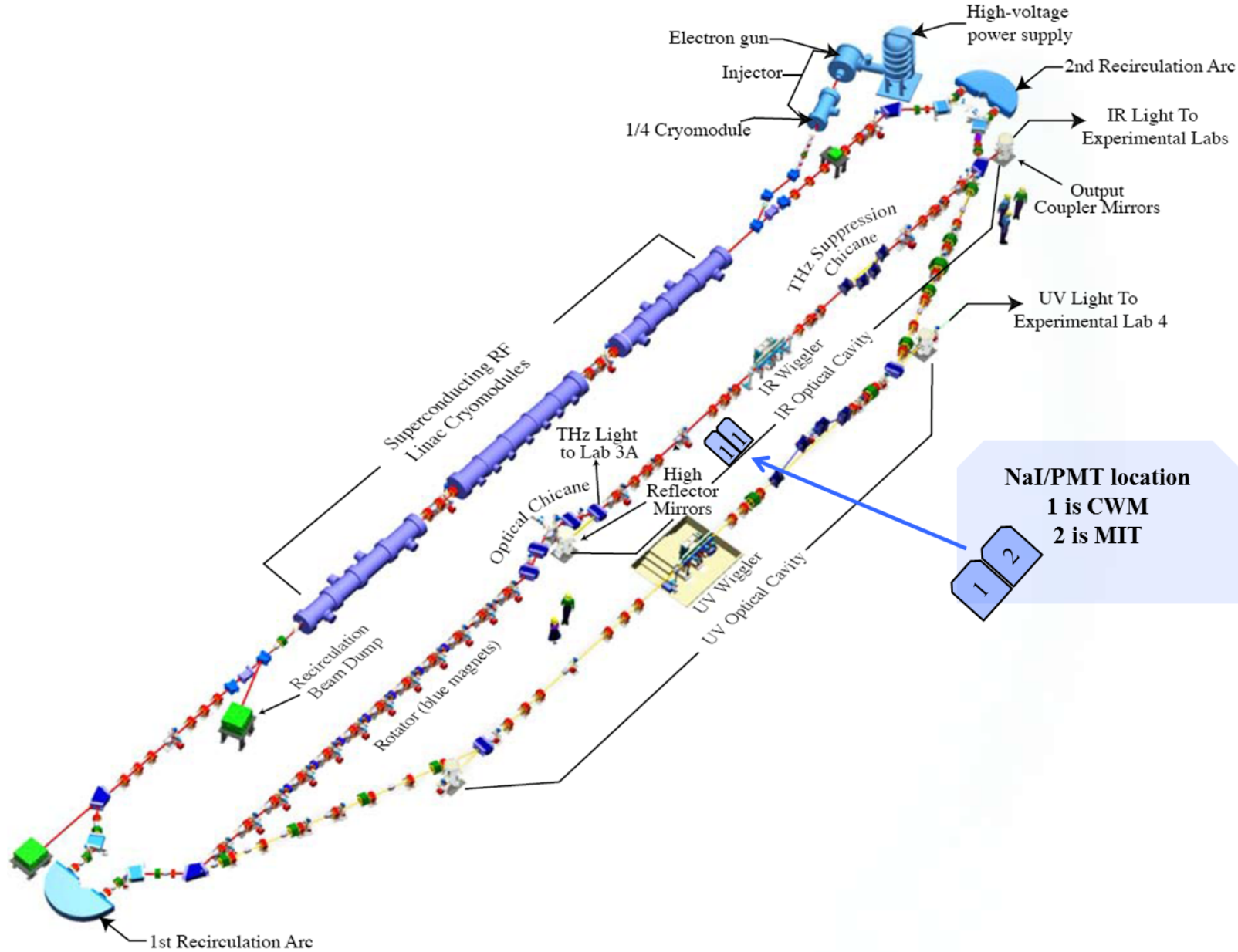


FIG. 11: Location of the two NAI/PMT detector setups near the IR line in the FEL vault.

on. A number of data runs were taken under varying beam conditions. (See Table I.)

3. Summary of radiation measurements

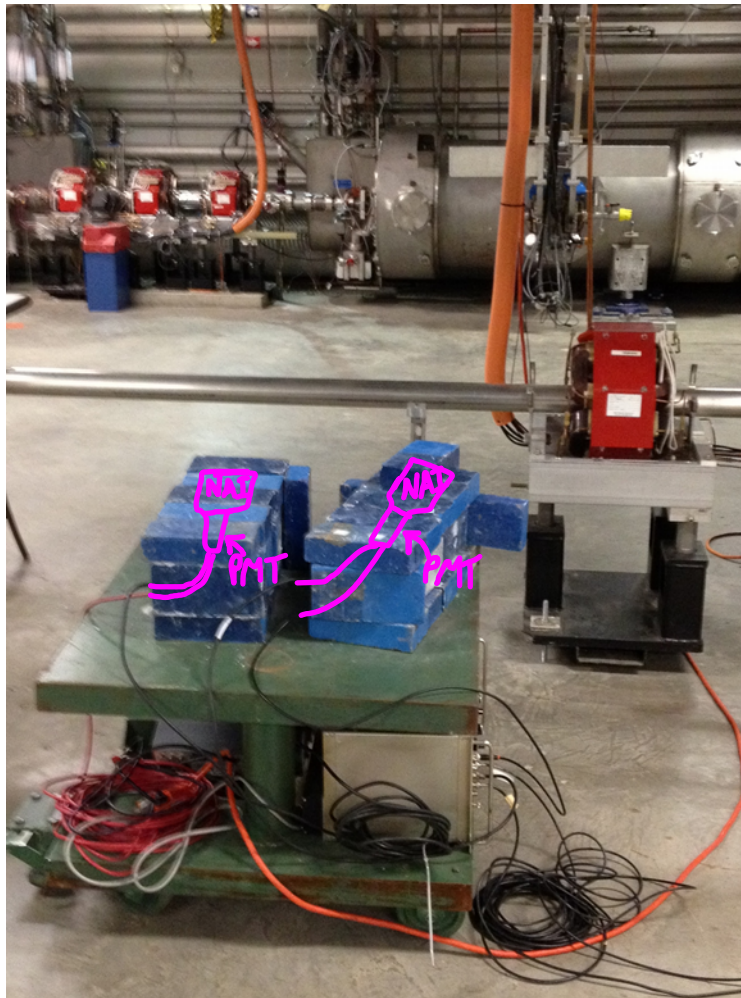
In summary, the radiation measurements carried out to date in the FEL vault indicate the presence of a significant photon and/or neutron background in the range from a few

Run # range	Pb config.	Beam/RF	MIT ($\times 10^5$)	W&M ($\times 10^6$)	Ratio
002–003	4" shielding	0.6 mA	9.32	6.14	0.152
004–007	4" shielding	1 mA	9.17	6.51	0.141
008–010	4" shielding	RF only	7.04	4.97	0.142
011–013	6" shielding	0.6 mA	4.24	5.07	0.0836
014–017	6" shielding	1 mA	4.95	5.64	0.0878
018–020	6" shielding	RF only	3.56	4.23	0.0842
021–023	2" shielding	0.6 mA	24.1	5.54	0.435
024–026	2" shielding	1 mA	26.3	6.08	0.433
027–029	2" shielding	RF only	18.7	4.35	0.430
030	2" shielding PMT HV off, 0.6 mA		0	0	N/A
033	2" shielding PMT HV off, RF only		0	0	N/A

TABLE I: Running conditions investigated for the background measurements study. Data was taken on owl shift, April 24, 2012. Three runs were taken at each shielding/beam/RF combination and summed. The “MIT” column lists count integrals from approx 250 keV to 2 MeV spectra in the NAI/PMT setup whose shielding was varied. The “W&M” column lists integrated counts in the same energy range for the normalization detector (2 inches Pb). The last column is the ratio.

keV up to a at least several MeV. Continued studies are underway. Goals are to determine the relative contributions of neutrons vs. ~~photons~~ ^{Extra space} photons and to study the effects of making the shielding more hermetic, ~~providing~~ ^{Which would provide} ~~providing~~ ^{providing} 4π coverage.

It has been noted during these tests that backgrounds can vary by an order of magnitude or more under otherwise similar running conditions in terms of beam current, pulse rate, etc. It may be that significant reduction of backgrounds is possible by careful choice of operating conditions by tuning of the beam, RF, and other beamline components during dedicated ~~runing~~ ^{running} for DarkLight. Still, it seems that some shielding for the detector may well be required.



It might be useful to show how the NAI detector is situated in the lead

FIG. 12: Pb enclosures (blue) housing the two NAI/PMT detectors near the IR line. Cryo module FL02 is in the background.

IV. EXPERIMENTAL DESIGN

V. EXPERIMENT DESIGN

Why two titles?

In this section, the conceptual design of the DarkLight detector and target are described. The goal is to measure elastic electron proton scattering below pion threshold using the 100 MeV electron beam of the JLab FEL. With 10 mA of electron beam incident on a windowless gas target of thickness 10^{19} hydrogen atoms/cm², a data taking luminosity of 6×10^{35} cm⁻² s⁻¹ is attained. In 60 days of 100% efficient data taking, an integrated

Again, this seems really optimistic to me

We just need the plots and axes -- why include all the rest of the window mess?

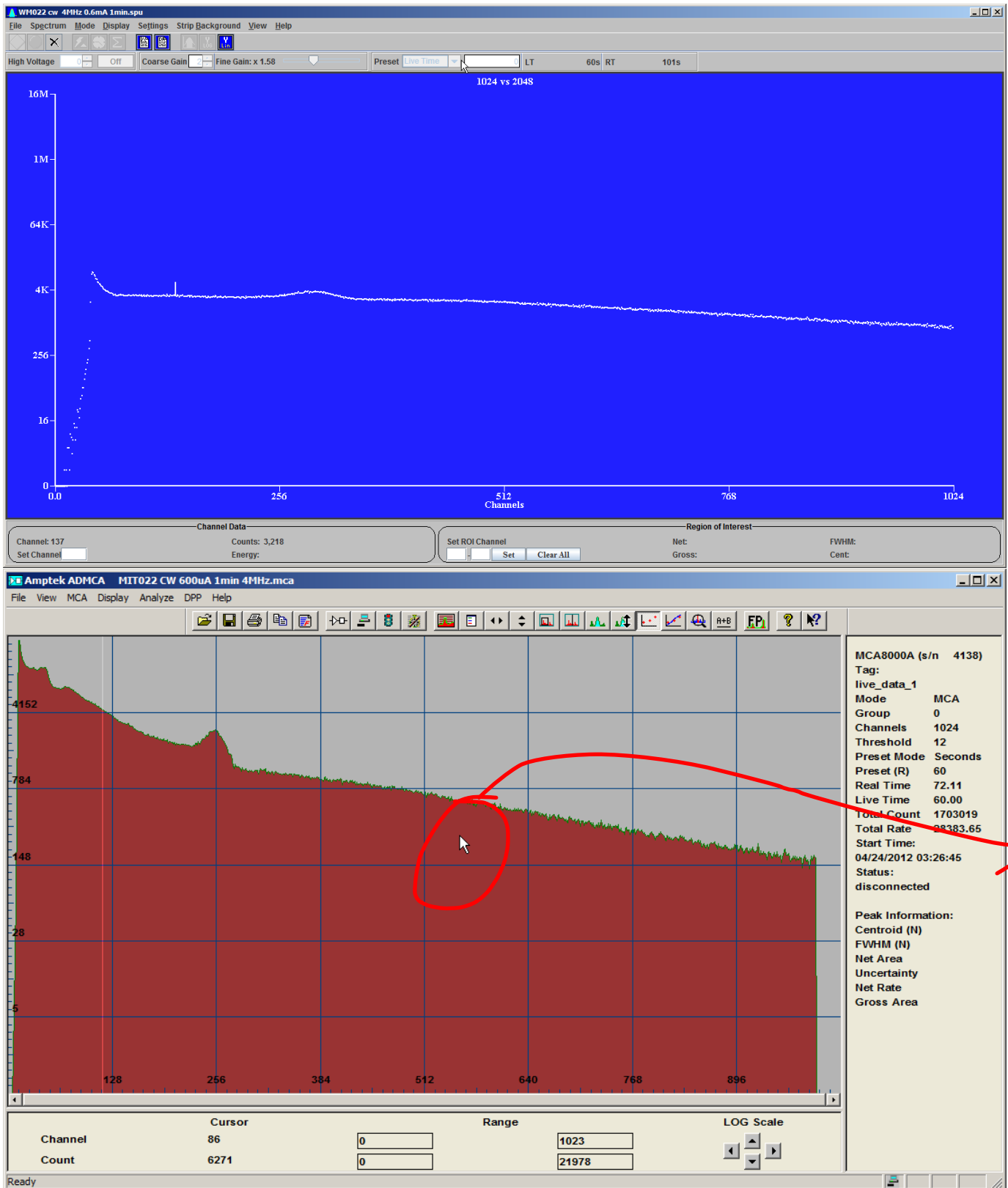


FIG. 13: Sample spectra taken by both NAI detectors: W&M (top), MIT (bottom). These were for run #022 in Table I. The bump approximately 1/4 from the left is near 511 keV.

Would it make more sense to highlight the bumps a different color and refer to it that way?

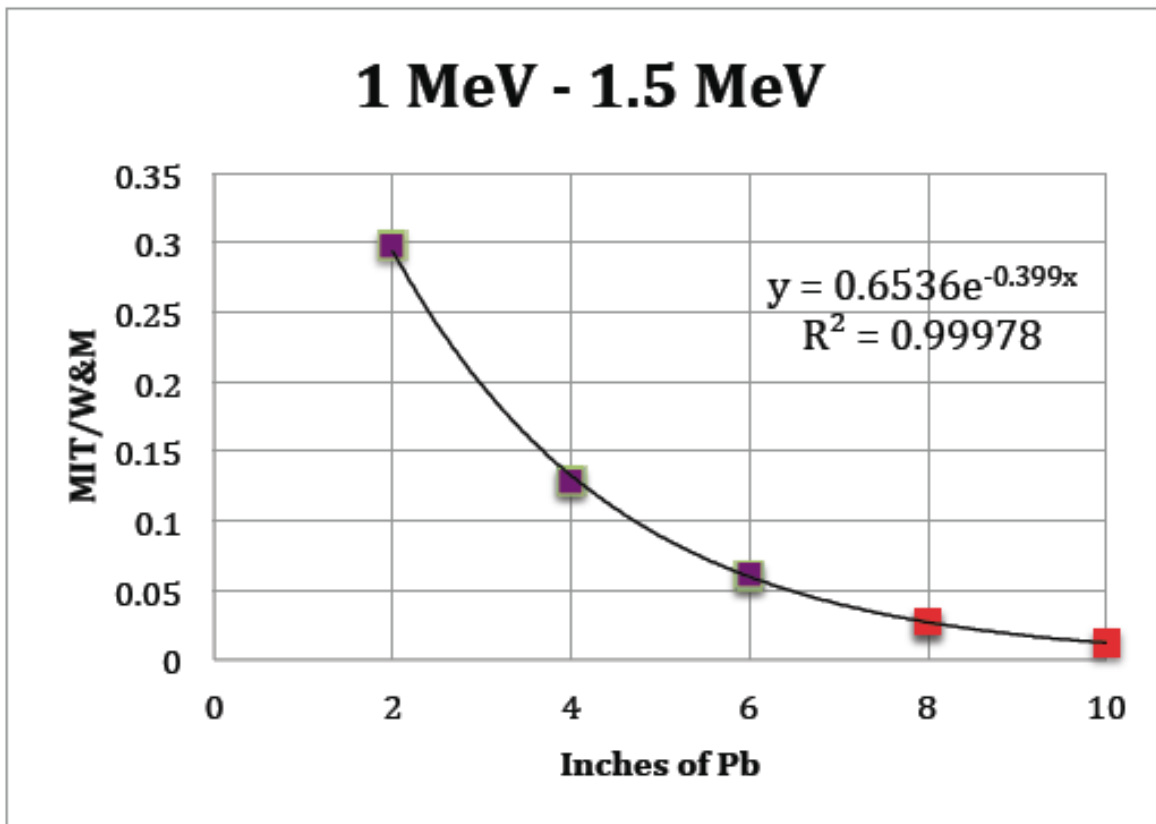
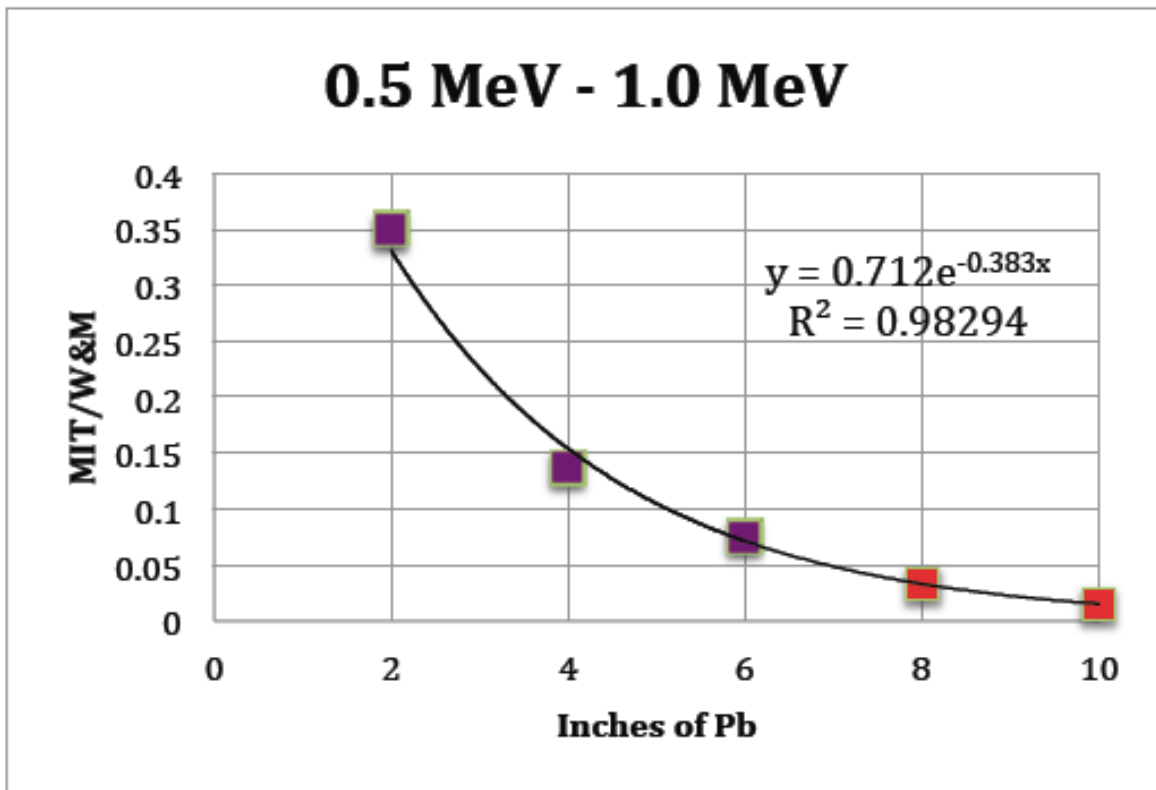


FIG. 14: Additional Pb shielding configurations: four inches on top, sides, and front (left) and six inches (right). The reference detector used for normalization is in the rear two inch thick enclosure, the other detector in the front enclosure.

luminosity of 1 ab^{-1} is acquired. The experiment is designed to detect in coincidence with high efficiency the scattered electron, the recoil proton and the produced positron-electron pair. The identification of all the final state particles allows the determination of the full event kinematics and efficient background rejection. The design of the DarkLight experiment is guided by the experience of members of the collaboration with the BLAST experiment at MIT-Bates [? ?] and the OLYMPUS experiment now taking data at DESY [?].

Since the submission of the DarkLight proposal [?] in November 2010, the design of the experiment has been significantly revised. In particular, the high rate of Moller scattered electrons in the forward direction demanded a longitudinal magnetic field of order 0.5 T to direct them out of the acceptance of the detector. Thus, the magnetic field used to track the final state leptons is now a solenoidal of magnitude 0.5 T . Shielding the lepton tracker from the large rate of associated radiative Moller photons requires a significant amount of

Why is T italicized?
No other units are

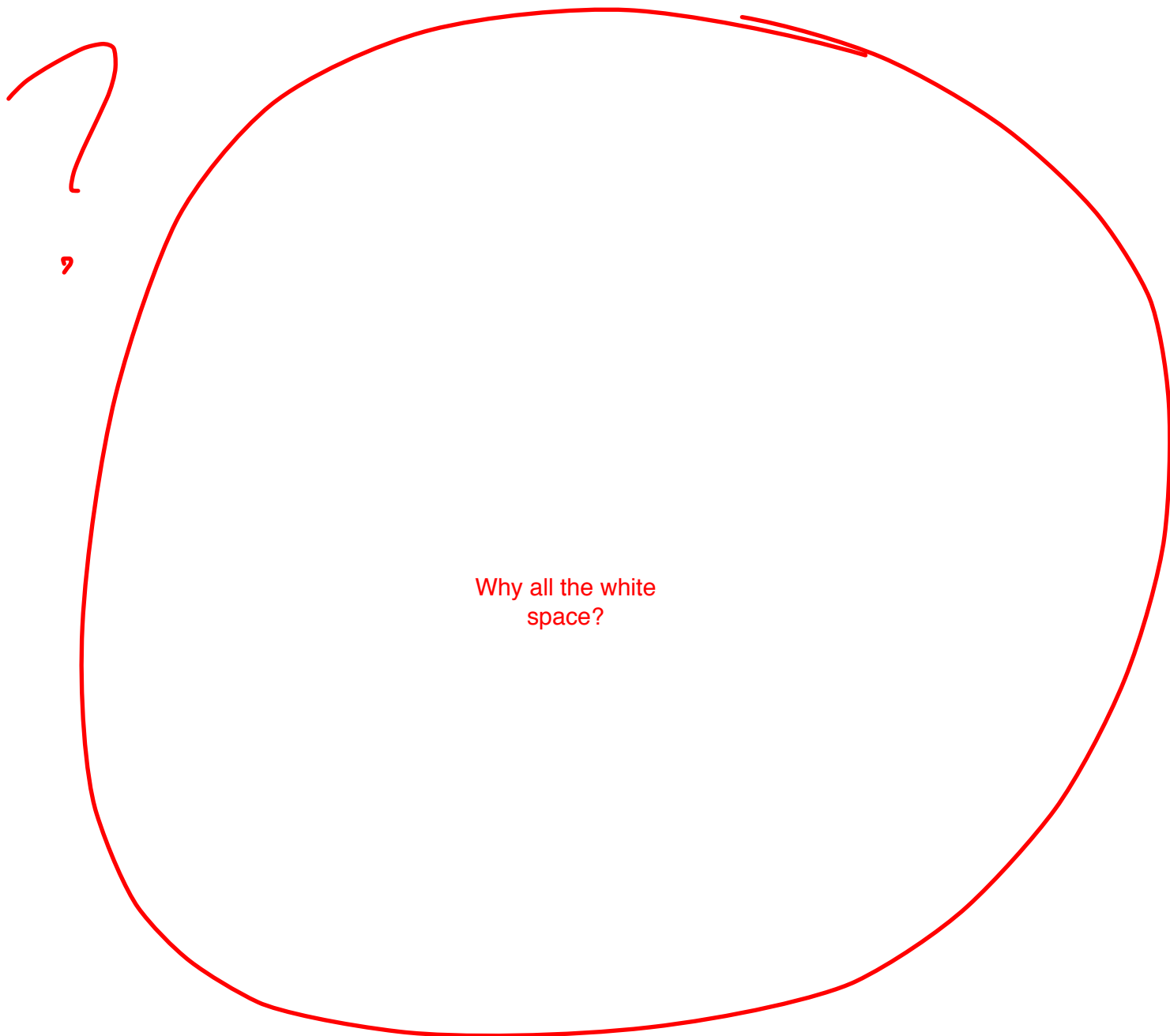


What's the error bars on these? Also, these plots are huge for having so few data points! Why not put them side-by-side instead? Also (aesthetic note), the shadows make it look tacky

Where's the rest of the caption?

FIG. 15: Normalized counting rates (purple points) for the three different Pb shielding configurations, summed over running conditions (RF only, 0.6 mA beam, 1.2 mA beam). Curves are fitted

shielding downstream of the target. The choice of technology for the lepton tracker is the GEM-TPC designed and built by a German collaboration [?]. An inner silicon detector will be used to detect the recoil proton from elastic scattering as well as provide tracking for the final state leptons.



A. Design considerations

TABLE II: Detector specifications for the DarkLight experiment.

Incident electron energy	100 MeV
A' mass range	10 to 100 MeV
Scattered electron angle	25° to 165°
Final electron energy	5 to 100 MeV
Recoil proton kinetic energy	1 to 6 MeV
Experimental A' mass resolution	1 MeV
Total elastic rate within detector acceptance	10 MHz
QED trigger rate	1 kHz

Title and caption located differently here from other tables

1. Elastic scattering rate

Elastic scattering presents the major process and a significant source of background. The cross-section for elastic electron-proton scattering can be written as

$$\frac{d\sigma}{d\Omega} = \frac{4\alpha^2 E'^2 \cos^2 \frac{\theta}{2}}{\sin^4 \frac{\theta}{2}} \cdot \left[\frac{G_E^2 + \tau G_M^2}{1 + \tau} + 2\tau G_M^2 \tan^2 \frac{\theta}{2} \right]$$

where $\tau = \frac{Q^2}{4M^2}$ with M the proton mass; $G_E(Q^2) = [1 + Q^2/0.71\text{GeV}^2]^{-2} \approx 1$; $G_M(Q^2) = 1.79 \cdot [1 + Q^2/0.71\text{GeV}^2]^{-2} \approx 1.79$.

May want to clarify GEp and GMp -- the fits aren't quite the same for GEN and GMn (4)

The elastic electron-proton cross-section has been calculated as a function of θ and the rate into bins of $\pm 2.5^\circ$ in θ and covering 2π in azimuthal angle, i.e. $\Delta\Omega = 2\pi \sin\theta\Delta\theta$ determined. A luminosity of $6 \times 10^{35} \text{ cm}^{-2} \text{ s}^{-1}$ has been assumed. The angle that the recoil proton makes with the incident electron beam θ_q is also calculated for each value of θ . The rates are summarized in Table III.

2. Møller scattering rate

The Møller process, i.e. the scattering of beam electrons on target electrons, produces an enormous rate of scattered electrons which might overload the detectors. A calculation

electrons

This could be worded better

θ deg.	E' MeV	T_p MeV	Q^2 (MeV/c) ²	$\sin^2 \theta/2$	θ_q deg.	rate MHz
15	99.6	0.4	677	0.017	82.5	148
30	98.6	1.4	2642	0.067	77	17
45	97.0	3.0	5665	0.146	66	5
90	90.4	9.6	18080	0.5	42	0.3
135	84.6	15.4	28899	0.854	21	0.2
155	83.1	16.9	31677	0.953	11	0.06

Minor thing -- this might look better wider with the units in parentheses next to the quantities instead of under them

TABLE III: Kinematics and rates for elastic electron-proton scattering in the DarkLight experiment. E' is the scattered electron energy, θ is the angle with respect to the electron beam direction and θ_q is the angle the recoil proton momentum vector makes with the beam axis.

of the expected count rate for 1° wide detectors with 2π azimuthal coverage is shown in Fig 16.

As can be seen in Fig. 17, the momenta of electrons scattered at larger angles are very small and these electrons will not exit the target volume. At smaller angles, the electrons will be bent around the beam line by the solenoidal field so that they will not reach the detector elements.

bent

Is the field in the shape of a solenoid or caused by it?

The next leading electromagnetic process, i.e. internal radiation, gives rise to photons with a bremsstrahlung $\frac{dk}{k}$ spectrum with an angular distribution similar to Møller scattering. The total radiated Møller photon rate is estimated to be of order 0.5% of the Møller rate. These photons must not be allowed to interact with the lepton tracker.

Extra space

How are we stopping them?

3. QED background rate

Again, make sure notation stays consistent

The QED background process $e^-p \rightarrow e^-pe^+e^-$ represents a smooth, irreducible background process for DarkLight on which the peak representing the decay of the A' is sought. It has been calculated in detail in [?] which has been used extensively in the design described in this proposal. For example, the QED trigger rate within the acceptance of the detector described here is estimated at about 1 kHz, which is a manageable rate.

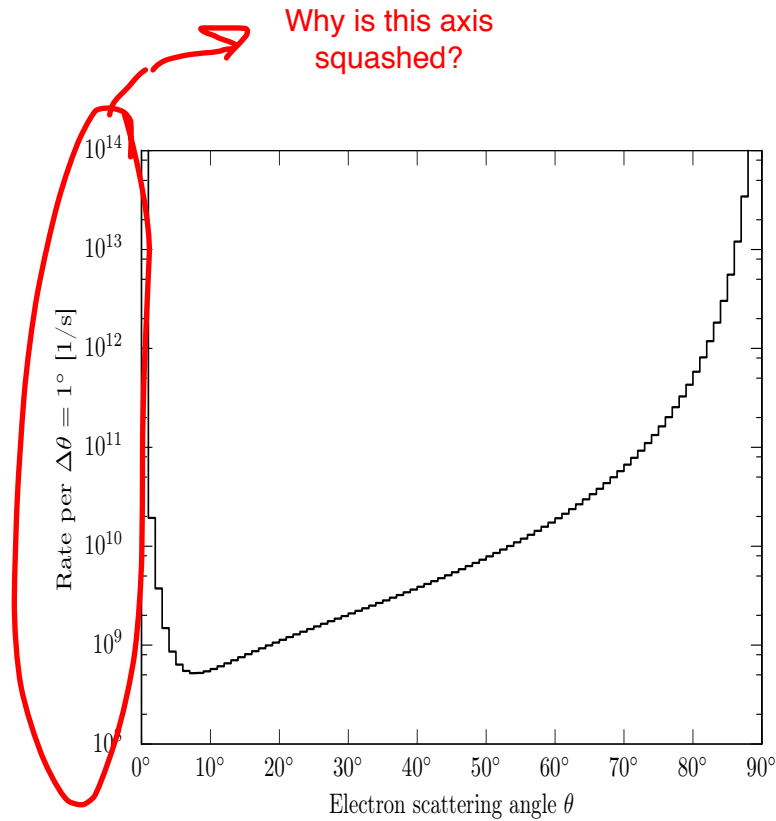


FIG. 16: The rate of Møller electrons on a 1° detector with 2π azimuthal coverage for the design luminosity of $6 \times 10^{35} \text{cm}^{-2}$ and an incident beam energy of 100 MeV.

4. Summary of design constraints

The DarkLight detector must be able to detect with high efficiency an electron-positron-proton final state in the presence of a large QED background rate. This leads to a number of design constraints as follows:

Inconsistent with T above

- A magnetic field is required to both provide an invariant mass resolution of order 1 MeV and to shield the detectors from background process, e.g. Møller scattering and showering from halo particles. The longitudinal field of magnitude 0.5 Tesla is provided by a normal conducting solenoidal magnet. The solenoid will accept all scattered electrons from 25° to 165° .
- Leptons from 5 MeV to 100 MeV must be tracked within the toroid. A cylindrical GEM-TPC will be used to track the leptons. In addition, a scintillator hodoscope will be configured outside of the cylindrical tracker.
- The target will be a windowless storage cell with three stages of differential pumping

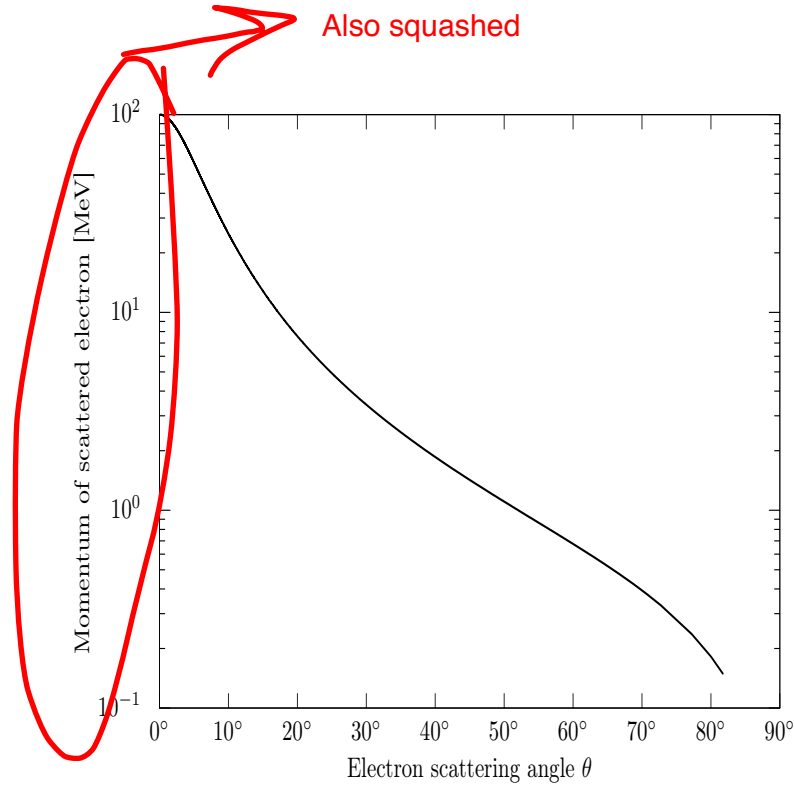


FIG. 17: The momenta of Møller electrons as a function of the scattering angle for an incident energy of 100 MeV.

on each side of the target. The silicon recoil proton detector will be located inside the gas volume.

- The final state proton will have a kinetic energy from about 1 to about 5 MeV. A 50 μm thick silicon layer followed by a 300 μm layer will be located around the gas target to detect the low energy, recoiling protons. This will be in the trigger at a high level.
- The elastic rate peaks in the forward direction for the final-state electron and at around 90° for the final state proton. By building a detector with no electron acceptance forward of 25° one would reduce the elastic rates very significantly. The minimum angle of detection needs to be determined in the context of maximizing the signal-to-noise. Correspondingly, the recoil proton rates are peaked at angles $\approx 90^\circ$. The recoil protons from events where an e^+e^- pair is produced are all located forward of about 60° - see top right panel of Fig. 14 from [?]. **Figure 14 is of the NAI detectors**
- The total elastic electron-proton rate for a detector with electron detection only for $\theta > 30^\circ$ and for proton detection $\theta_q < 60^\circ$ is of order a few MHz from the above table.

B. Magnet

To meet its physics goals, DarkLight requires a magnet to assist in the tracking detection of charged particles. In addition, a magnetic field is required to shield the detector from the very high rate of very low energy background electrons. A solenoid around the beam line and enclosing the detector elements can provide a longitudinal field of sufficient strength to both mitigate the background and allow for momentum analysis of charged leptons. An iron-type yoke around the solenoid is needed to provide a flux return. This in turn can substantially improve the field uniformity over the detection volume and can be used as part of the mechanical support of the solenoid. In the DarkLight pre-proposal, a toroidal magnet was also considered as a design option. Although a toroid meets the field requirements in the detection region it would require the addition of a holding field around the target region to block the low energy background. Thus the adoption of the solenoid with a yoke return is seen as the most appropriate choice, one that will require a careful mapping of the magnetic field in the region of interest.

The magnetic field strength of the solenoid is chosen to be 0.5 T in order to trap most of the low energy background and allow electrons and positrons of interest to reach the detection region. The solenoid inner radius has to start around 30 cm from the axis to accommodate for the target and the detector elements. A preliminary design of the solenoidal magnet surrounding the target region is shown in Figure 18 where dimensions are given in mm. A cylindrical yoke 10 cm thick, with two end caps, and an inner radius of 50 cm is proposed to be made of C1010 steel.

The characteristics of the copper conductors chosen for this design are listed in Table V. These conductors are commercially available and approximately half the area of the conductor is used for the water cooling bore.

Table VI lists some of the yoke dimensions and the parameters that characterize how the conductors are arranged to form the solenoid coils. There are seven coil layers, each layer has 67 loops along the axis of the solenoid yielding a solenoid length of 1.48 m. The total number of turns is $7 \times 67 = 469$ and the conductor total length comes out to be 1237 m.

Table VII lists some of the electrical and cooling main parameters. For a field strength of about 0.5 T the solenoid needs to be operated at a current density of about 516 A/cm² making it possible to cool the conductors using inlet water at room temperature. The mean

I would combine these two paragraphs

TABLE IV: Specifications for the DarkLight magnet.

Field	0.5 T
Yoke outside radius	600 mm
Yoke length	1700 mm
Yoke outside chamfer	100 x 100 mm x mm
Yoke inside chamfer	50 x 50 mm x mm
Coil inner radius	335 mm
Coil outer radius	490 mm
Coil length	1459 mm
Poletip hole radius	100 mm
Coil layers (radial)	7
Coil windings (long.)	66
Current	1274.6 A
Packing fraction	0.504
Coolant fraction	0.232 (m ³ water)/(m ³ coil)
Conductor	19.1 x 19.1 mm x mm
Cooling passage	12 mm

Height	Width	Corner	Cooling	Insulation	Total area	Conductor area
(mm)	(mm)	(radius)	(dia)	(thickness)	(mm) ²	(mm) ²
19.1	19.1	2.5	12	1.5	488.4	246.3

TABLE V: Dimensions of the normal conductors for the 0.5 T solenoid.

I would widen this to have only two lines in the title row instead of three

water temperature during operation is 35 °C. The power dissipated by the solenoid is 151 kW.

The solenoidal magnet of Fig. 18 has been modeled with the code OPERA. The solenoid was built using a single coil, 1.48 m long with inside and outside radii of 33.5 cm and 49.1 cm, respectively. The solenoid was surrounded by a cylindrical yoke made of steel C1010 with the dimensions as shown in Fig. 18. The magnetization curve used in the code for the material C1010 is shown in Figure 19. The magnet was located inside a cubic volume of

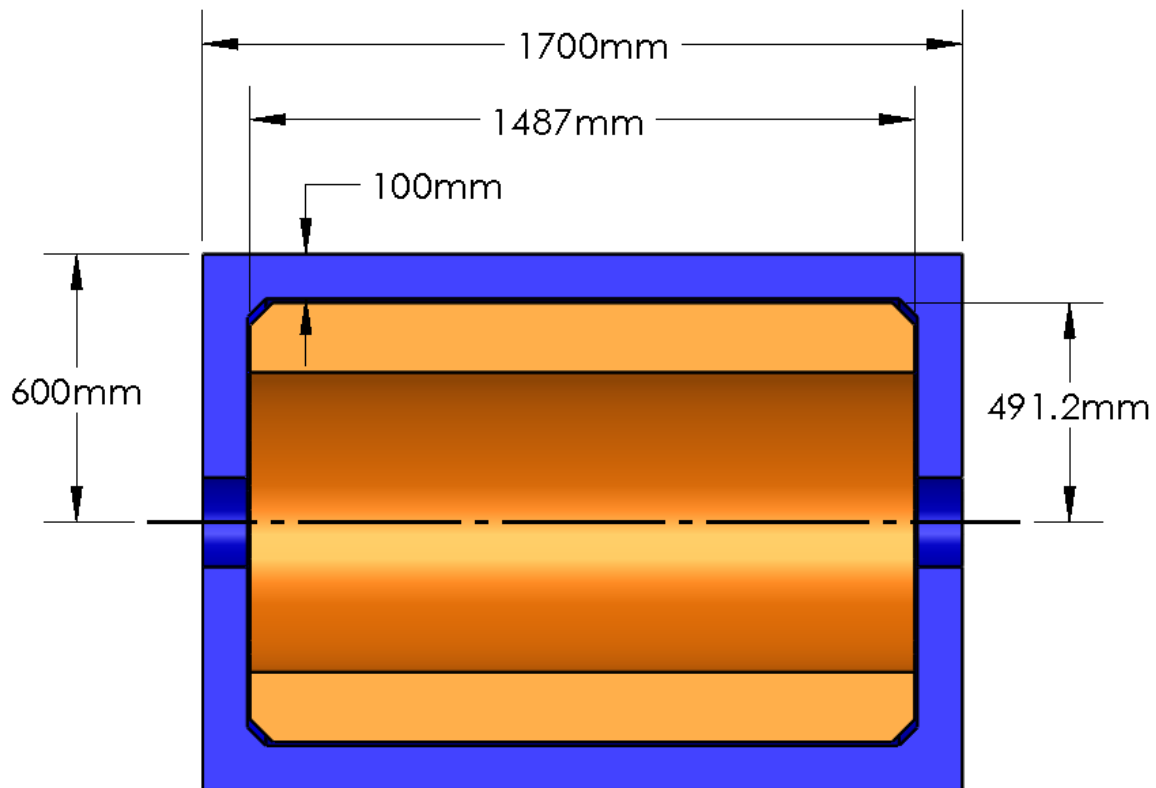


FIG. 18: Preliminary engineering concept of the solenoidal magnet.

Yoke (in/out radius) (m)	Yoke (length) (m)	Coil (layers)	Coil (length) (m)	Coil (loops)	Total turns	Conductor (total length) (m)
0.5/0.6	1.7	7	1.48	67	469	1237

TABLE VI: Yoke dimensions and conductor coil arrangements.

Current (A)	Flux (A-turns)	Resistance (series) Ohm	Voltage (V)	Power (kW)	T_{water} (in/out) (°C)	ΔP (per cooling path) (atm)
1273	597037	0.093	119	151	20/50	4.2

TABLE VII: Operational parameters for the 0.5 T solenoid.

Widen title row

27 m³. The current density was set to approximately match the parameters presented in Tables VI and Table VII.

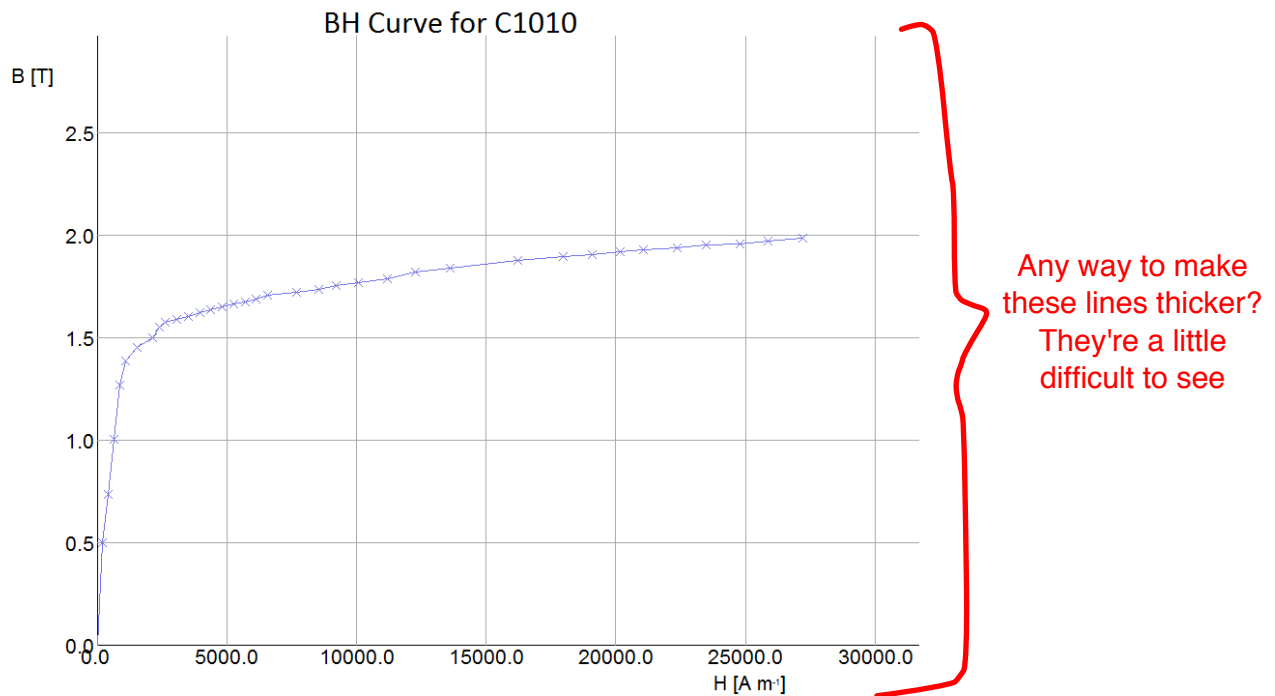


FIG. 19: Magnetization curve for steel C1010 as implemented in the code OPERA.

A view of the solenoid and the yoke is shown in Figure 20. Only a quarter of the yoke is shown to illustrate the interior. The color code on the yoke indicates the field strength ~~there~~ and the scale used is shown on the axis at the left of the figure. The figure on the right is a close up of the corner of the cylinder with the end cup and the field on this sharp corner of the yoke is very high bringing the yoke material close to saturation. To reduce this effect the proposed design as shown in Fig. 18 has a 45° cut around this sharp corner → What has a cut?

The magnitude of the magnetic field along the z-axis, i.e. beam line, is shown in Fig. 21. One curve shows the field due only to the coils while the most uniform curve is that obtained when the yoke is added to the solenoidal coil. The field is also very uniform over the detection region as can be seen in Fig. 22 that shows a color profile of the magnetic field magnitude on the *yz*-plane covering about 1.6 m along the beam line and about 1.2 m in the vertical direction. The field throughout most the yoke is constant, about 0.65 T, except → except on the sharp corners as already noted. In this regime the value of the field inside the yoke is very dependent on the sharp rise in the magnetization curve before saturation.

The trajectories of elastic scattering electrons from hydrogen have been calculated for the

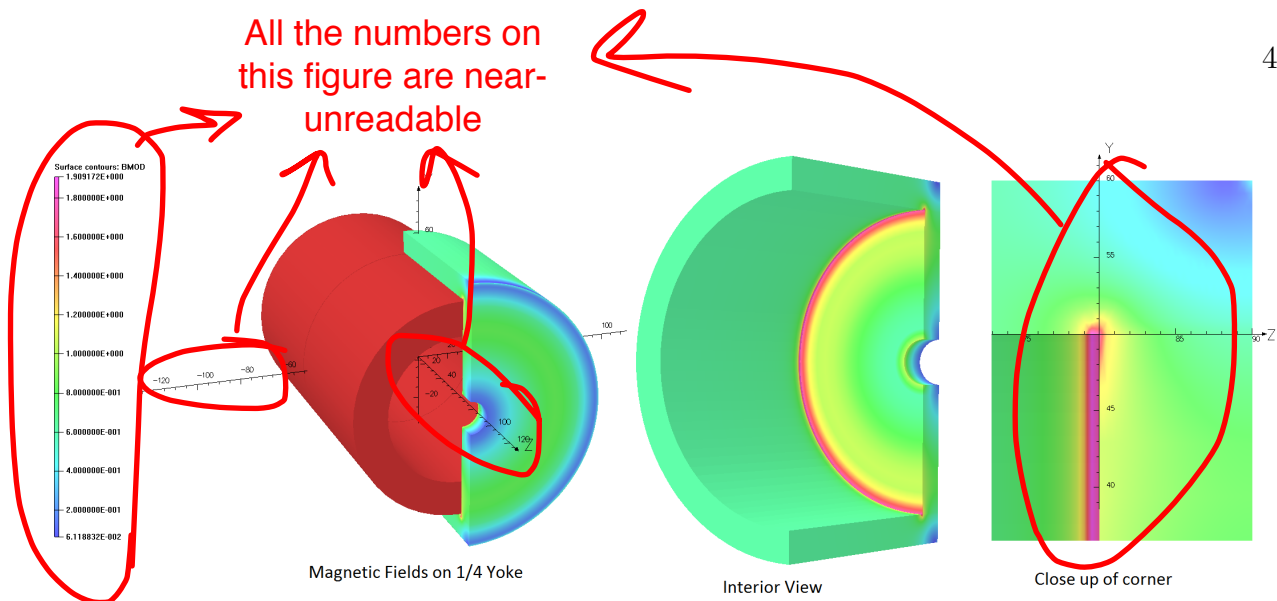


FIG. 20: The solenoid and the yoke as built in the code OPERA. The color code on the yoke represents field strength, the scale used is on the left. The picture on the right is a close up of the corner between the cylinder and the end cup of the yoke.

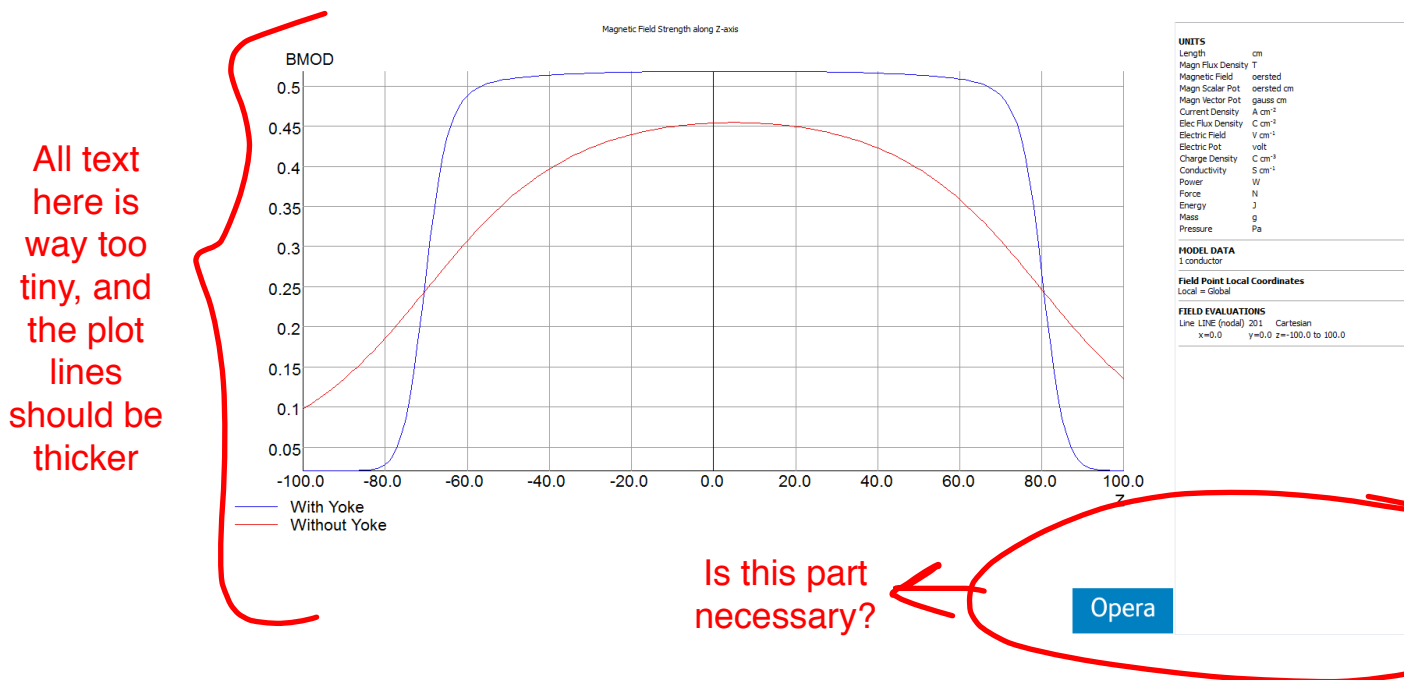


FIG. 21: Magnitude of the magnetic field along the beam line, field is in T and distances in cm. The curves are for the field with and without the yoke around the solenoidal coil.

above magnetic field configurations. The scattered electron angles and energies correspond to those from elastic scattering. The trajectories are shown in Figure 23 and are drawn in the $y-z$ plane, where y is the vertical direction and z the beam direction. Tracking electron detectors are expected to cover the entire z -range shown and the y -range between 15-35 cm

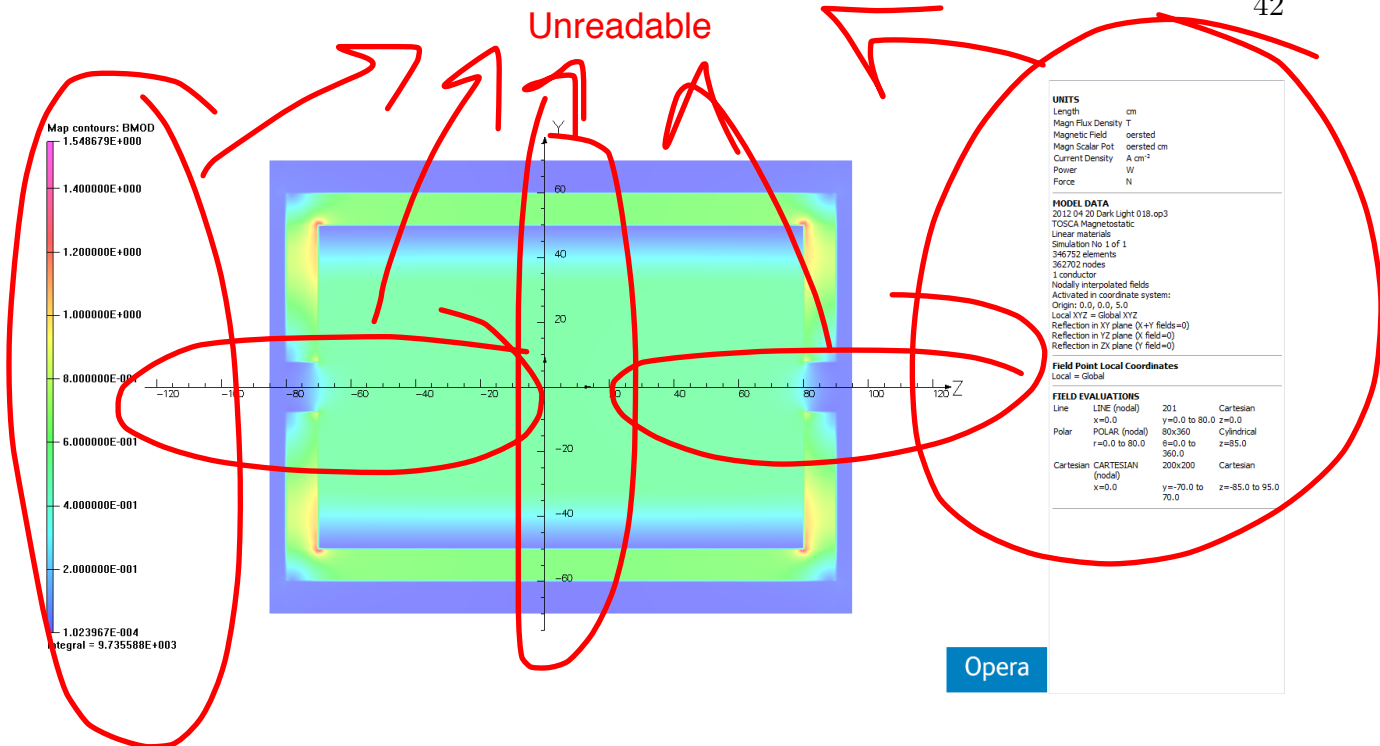


FIG. 22: Magnetic field profile on the yz-plane.

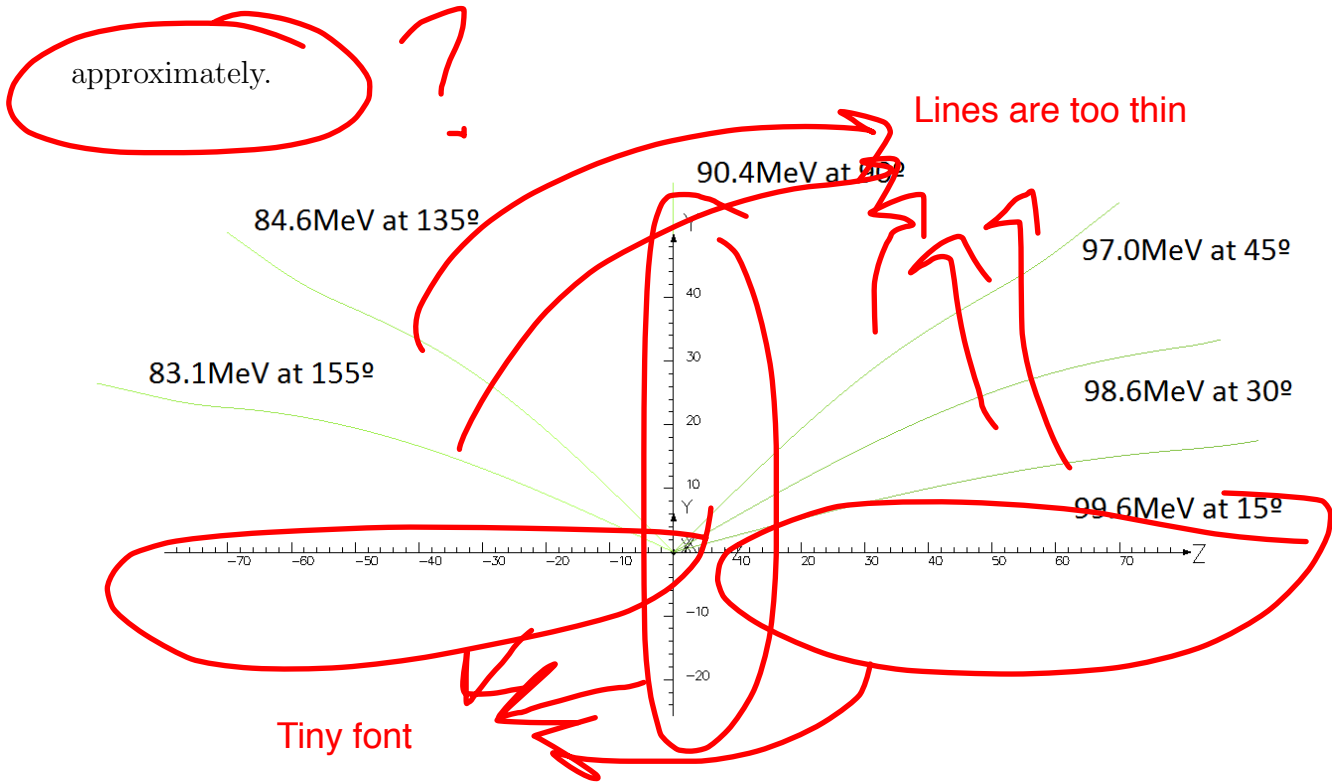


FIG. 23: Trajectories of electrons scattered elastically from hydrogen for a 100 MeV electron beam.

The DarkLight experiment requires the detection of the elastically scattered protons, whose energy are in the few MeV range, and the detection of electron and positrons within the 10-50 MeV range in addition to the elastic electrons. The proposed field does not affect significantly

the proton trajectories while allowing leptons of at least 10-15 MeV to reach past the 15 cm into the lepton tracking system. This is illustrated in Figure 24 for 1 MeV protons and in Figure 25 for 30 MeV electrons.

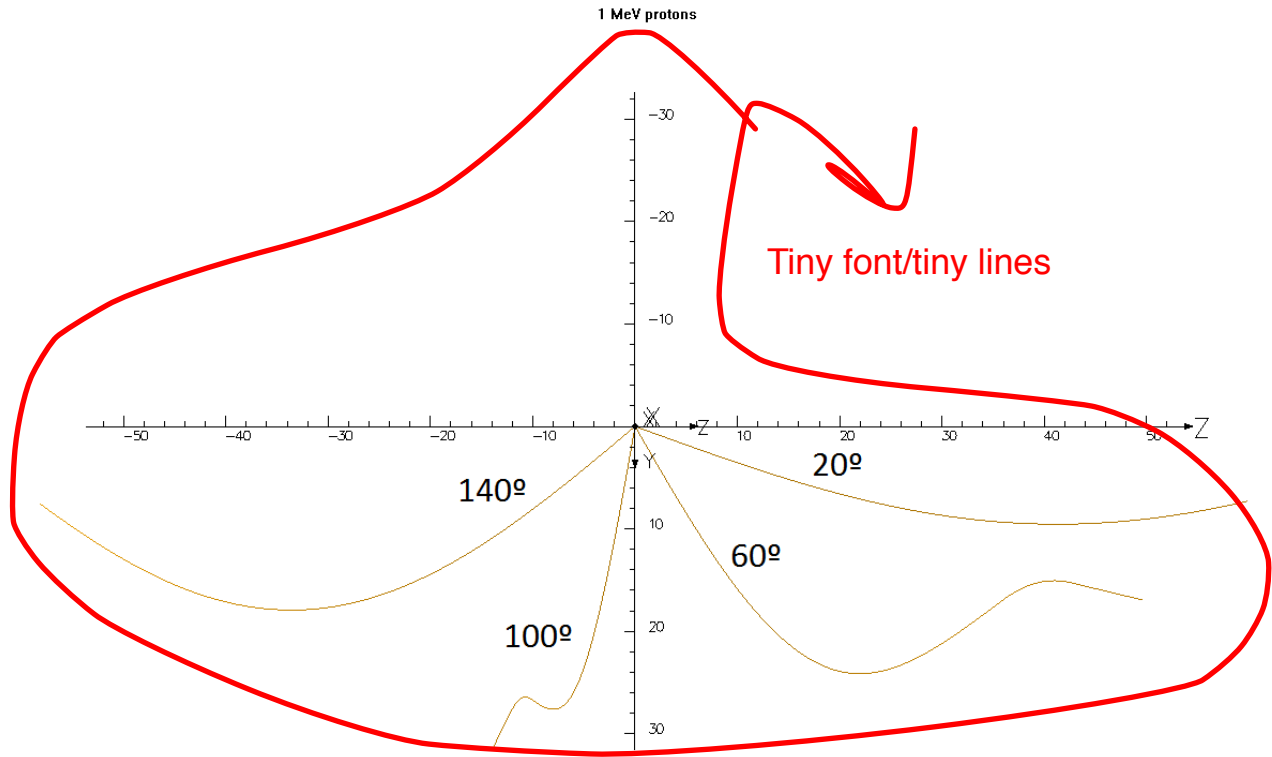


FIG. 24: Trajectories of 1 MeV protons as function of the scattering angle.

The design of the mechanical structure of the proposed magnet is driven by the weight of the entire device. The magnetic forces on the proposed coil configuration are about a tenth of the weight of the magnet.

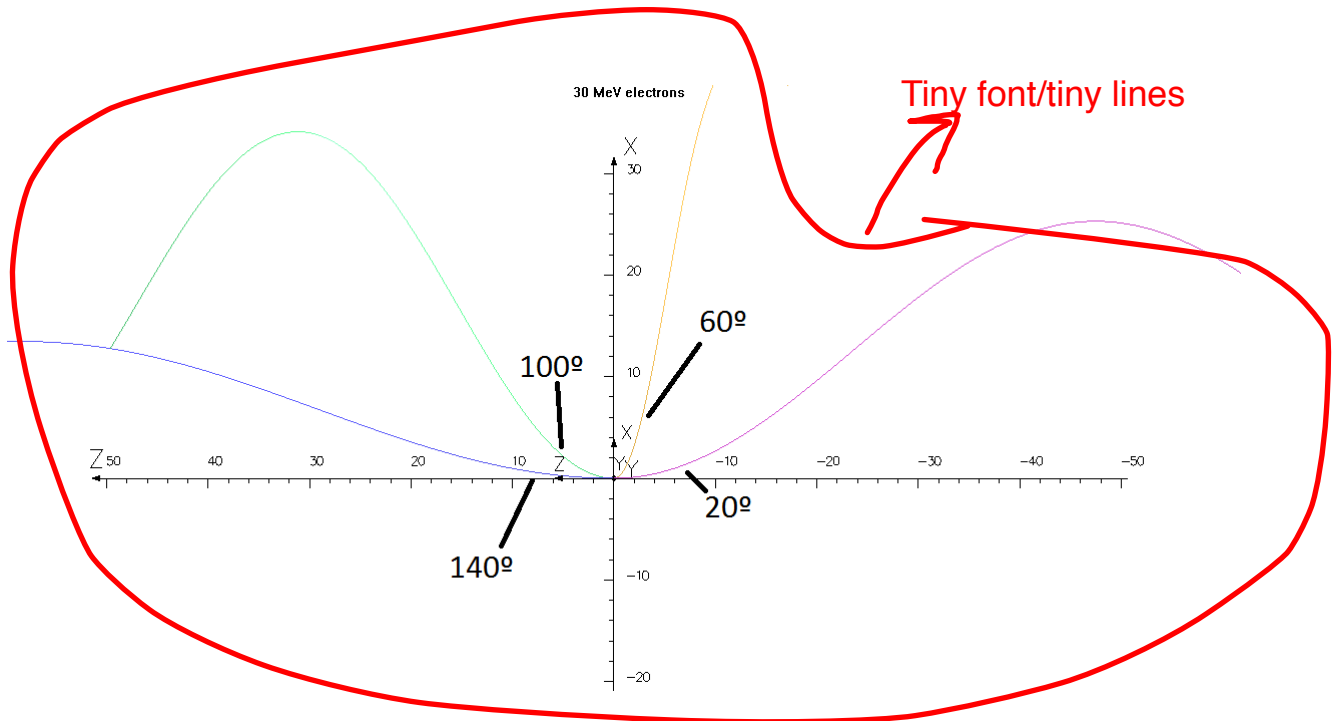


FIG. 25: Trajectories of 30 MeV electrons as function of the scattering angle.

C. Detectors

1. Lepton tracker

The lepton tracker in DarkLight must detect the final state e^- in coincidence with the e^+e^- pair from QED and via the A' decay. It must have the following characteristics:

- operate in a high rate (of order GHz) environment
- have low ($< 1\%$ rad. length) material thickness to provide 1 MeV resolution in the mass of the A'
- have cylindrical geometry in a solenoidal magnet
- provide a position resolution of $250 \mu\text{m}$
- trigger at a rate of about 1 kHz

The GEM-TPC developed by the GEM-TPC collaboration from Technische Universität München, HISKP Bonn, GSI Darmstadt, SMI Wien, and Universität Heidelberg [?], originally motivated by the proposed Panda experiment at FAIR, GSI, Darmstadt, Germany, is very well matched to the above requirements and is the proposed technology for DarkLight.

The GEM consists of a 50 μm thin insulating Polyimide foil with copper coated surfaces, typically 2 to 5 μm thick. The foil is perforated by photo-lithographic processing, forming a dense, regular pattern of (double-conical) holes. Usually the holes have an inner diameter of 50 μm . A large GEM-TPC prototype has been constructed, as shown in Fig. 26, and has been operated successfully [?]. It is a 60% scale prototype of the proposed DarkLight tracker and its characteristics are described in Table VIII.

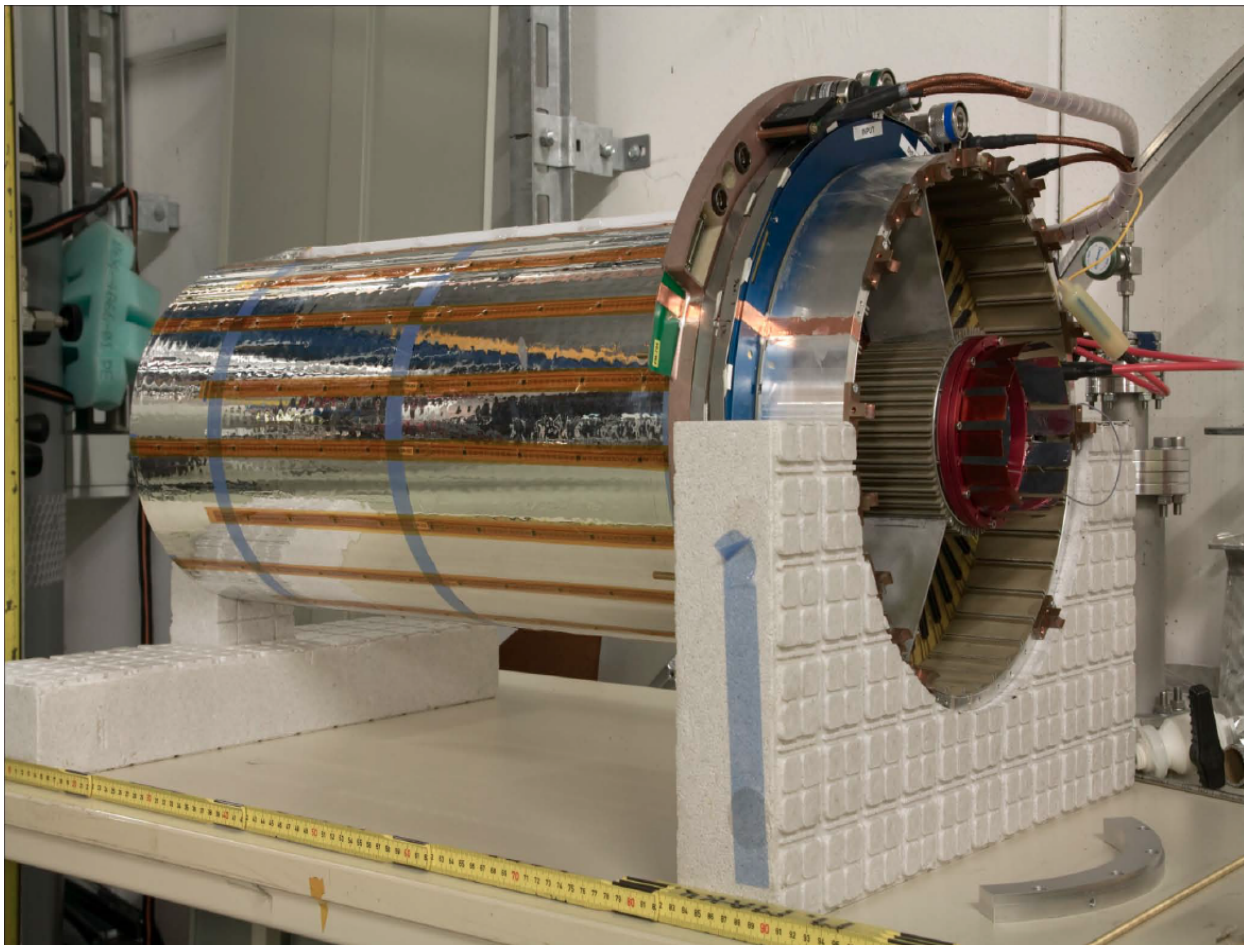


FIG. 26: Photograph of the prototype constructed by the GEM-TPC collaboration.

The GEM-TPC prototype material thickness satisfies the design requirements as shown in Fig. 28.

Combine paragraphs
 The GEM-TPC prototype has been installed in the FOPI detector at GSI and was used for data taking in 2011. It will also be used in the Crystal Barrel detector at ELSA, U.

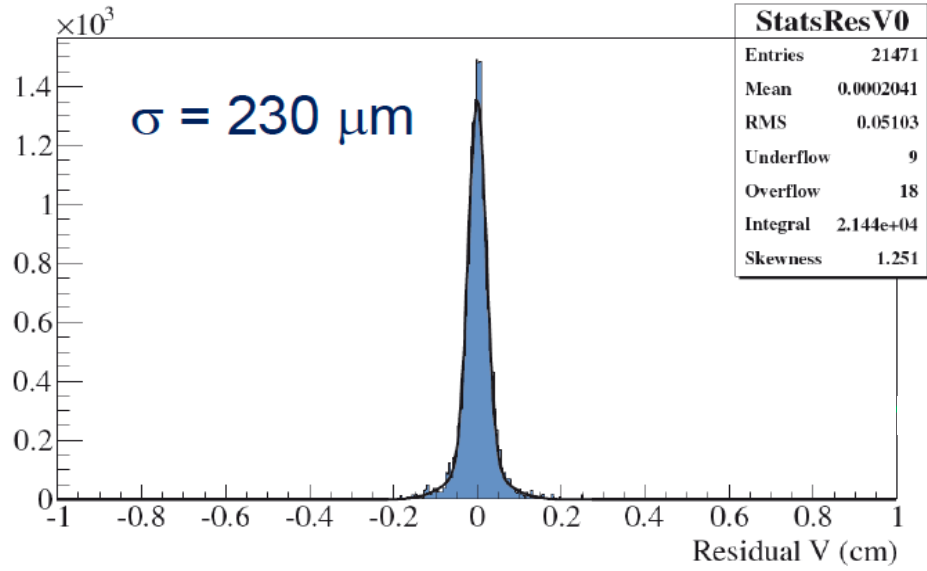


FIG. 27: Spatial resolution of the GEM-TPC prototype determined using cosmic rays. Here the field was 360 V cm^{-1} and the gain was 3700. The magnetic field was zero.

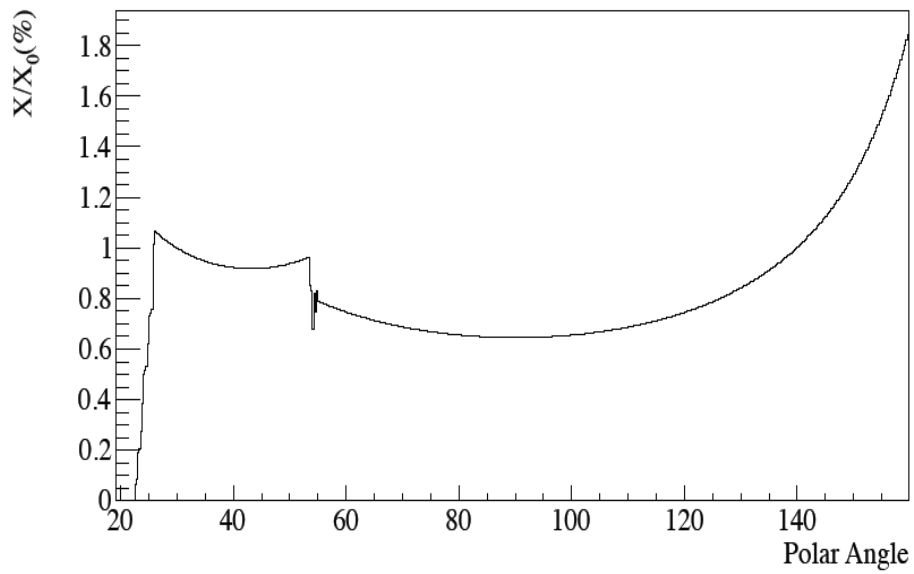


FIG. 28: Radiation length vs. polar angle for the GEM-TPC prototype [?].

TABLE VIII: Characteristics of the GEM-TPC prototype [? ?].

Drift length	725 mm
Outer diameter	300 mm
Inner diameter	105 mm
Triple GEM stack, gain O(1000)	
10254 channels	
AFTER T2K analog sampling readout	
Gas	Ar(Ne)/CO ₂ (90/10)
Position resolution (σ)	250 μ m

Bonn, Germany. The TPC operates continuously as an analog event pipeline. The readout electronics is based on the AFTER T2K chip and the sampling frequency is 10 to 50 MHz based on an external clock.

2. Inner silicon detector

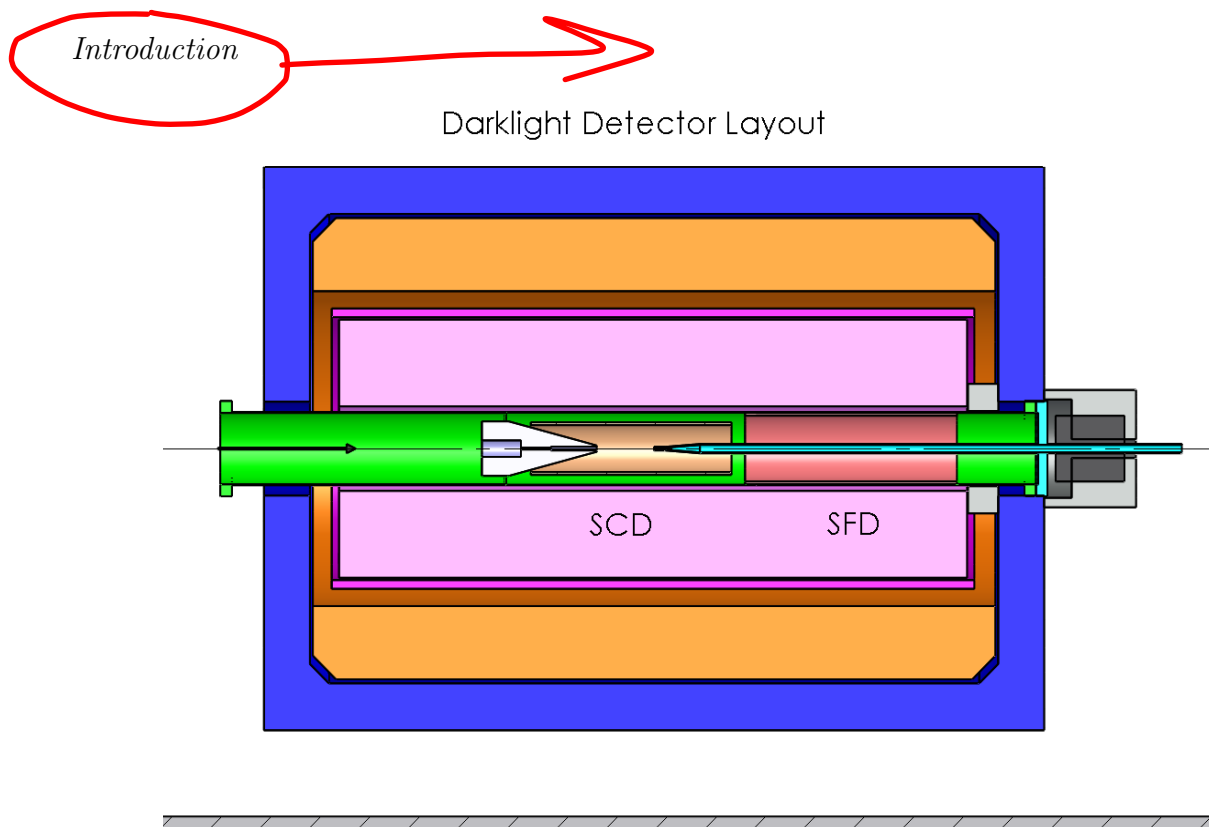


FIG. 29: Layout of the DarkLight experiment highlighting the location of the Silicon Central Detector (SCD) and the Silicon Forward Detector (SFD).

The silicon system of the DarkLight experiment serves two functions, the tagging and energy measurement of the recoil proton at the level of a few MeV in kinetic energy and the measurement of the hit location of final-state leptons. The layout is meant to aid the identification of recoil protons compared to final-state leptons. The silicon detector system is divided into two parts:

- Silicon Central Detector (SCD) (Polar angle range: $17^\circ - 163^\circ$)
- Silicon Forward Detector (SFD) (Polar angle range: $6.1^\circ - 19^\circ$)

Figure 29 shows the layout of the DarkLight experiment highlighting the location of both detector systems. The layout of this system is based on two independent sensors addressing

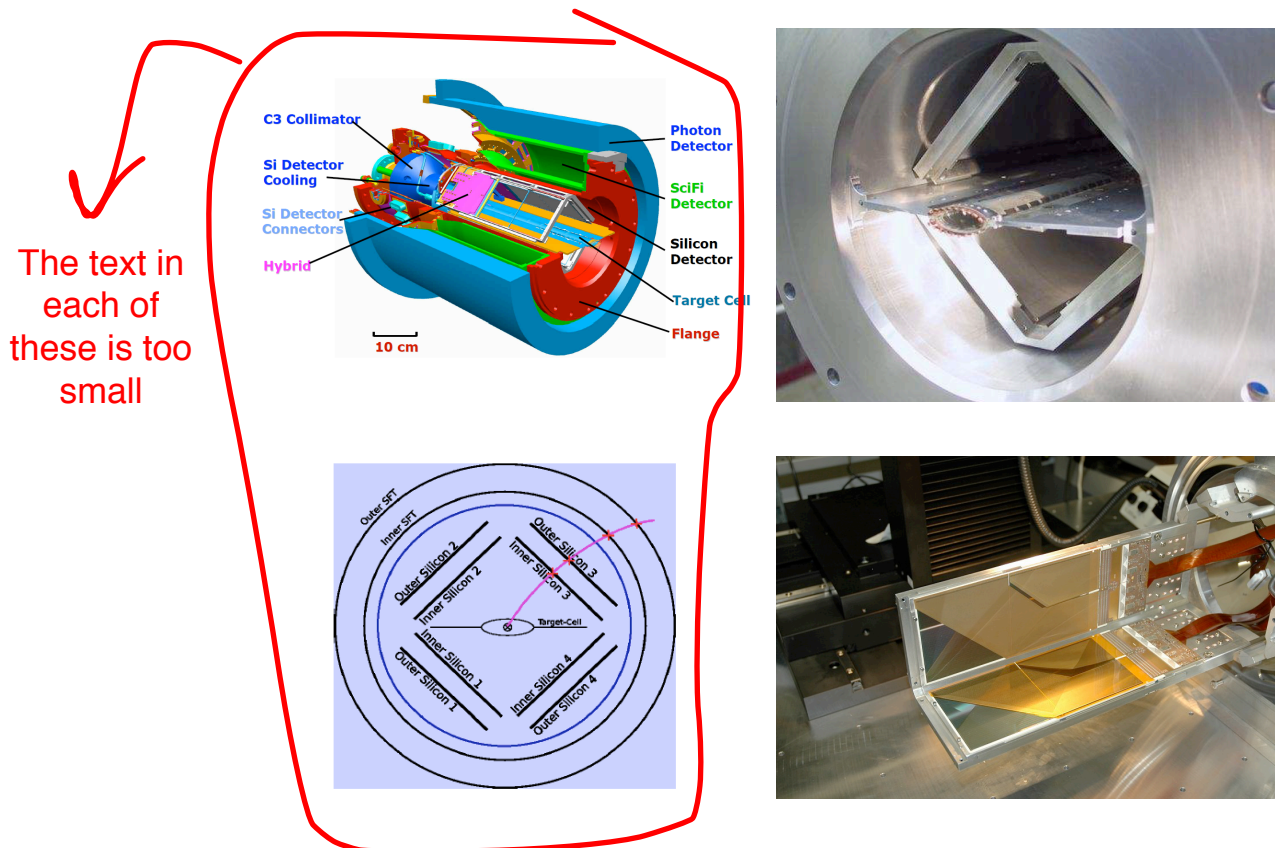


FIG. 30: Overview of the HERMES Proton Recoil Detector.

the need for recoil proton and lepton measurements covering rather different energy ranges. There are several examples of silicon sensor based detector systems focusing on measuring the energy and hit location of recoil nuclei such as the CNI polarimeter system at RHIC [?] and the proton recoil detector at HERMES [?]. Both silicon systems are operated inside the actual beam vacuum. Figure 30 provides an overview of the HERMES proton recoil detector. The silicon detector is based on four large double-sided silicon sensors stations each with two sensors referred to as inner and outer silicon. The silicon system for the DarkLight experiment is based on conventional, well-understood single-sided silicon sensors providing a robust silicon detector scheme while at the same time avoiding a long and costly R&D phase.

The first two sections discuss the requirements, followed by a description of the layout, the design concept and specifications. The last three sections focus on silicon ladder concept, the silicon sensors with a brief remark on the cooling system at the end.

Requirements → Formatting here is different from above

The DarkLight silicon detector systems, i.e. the SCD and the SFD (Figure 31), will be

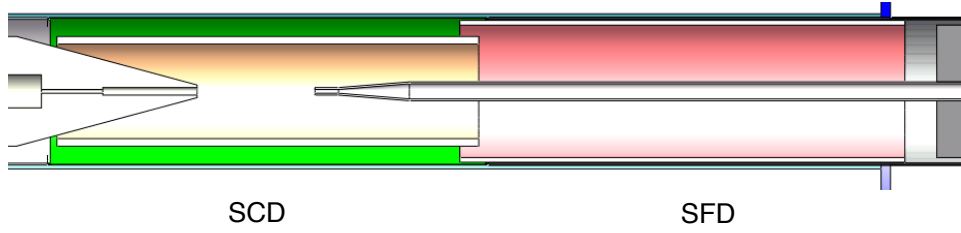


FIG. 31: Side view of the silicon-detector system for the DarkLight experiment with the Silicon Central Detector (SCD) and the Silicon Forward Detector (SFD).

operated inside the actual beam vacuum. This addresses in part the need for minimizing the dead material which is expected to stay below $1\% X_0$. A careful design on the choice of any support and service material is mandatory minimizing outgas rate. The following list summarizes all basic requirements:

- Central and forward measurements of recoil proton and final-state leptons covering a polar angle range of $17^\circ - 163^\circ$ and $6.1^\circ - 19^\circ$, respectively.
- Proton recoil energy and location measurement.
- Linearity in energy response for the proton recoil measurement.
- Hit location of final-state leptons.
- Dead material in active detector area below $1\% X_0$.
- Low outgas rate of any active and passive material.
- Radiation hard silicon sensors.
- Fast readout system to potentially contribute to the actual trigger system.
- Liquid cooled system of the chip front-end electronics.

Layout, Design concept and specifications

Figures 32 and 33 show a cross-section view of the SCD and SFD, respectively together with a list of basic design parameters. Figures 34 and 35 show a side view of the SCD and SFD, respectively.

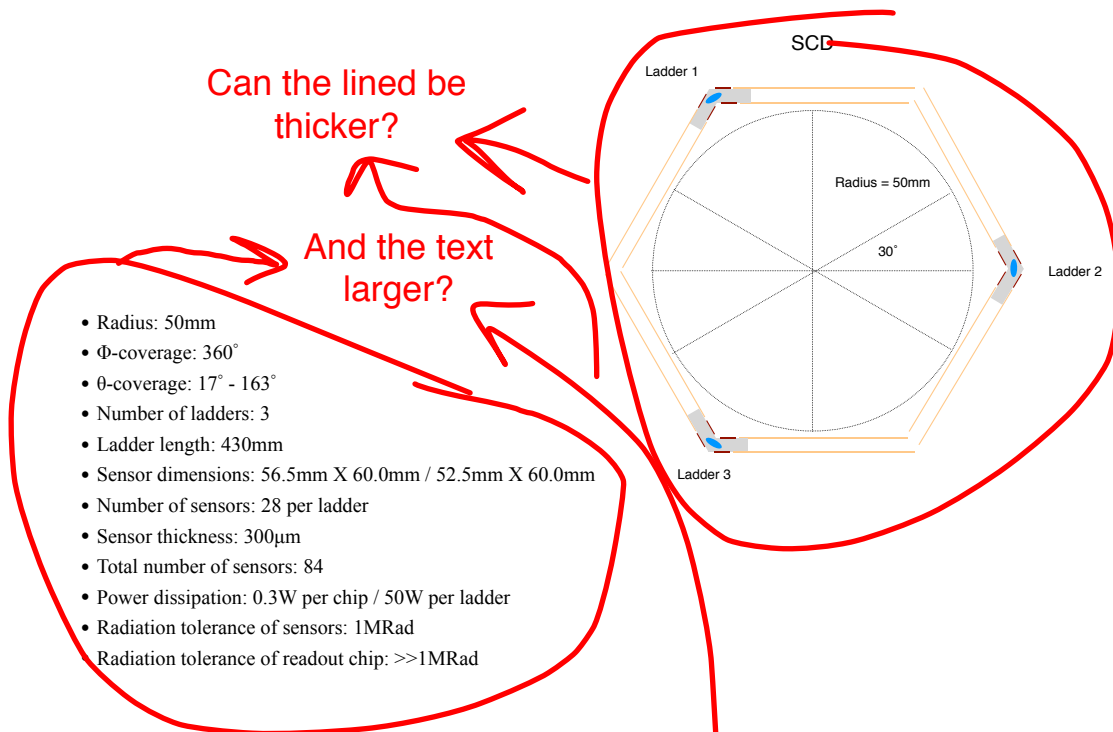


FIG. 32: Cross-section view of the DarkLight Silicon Central Detector (SCD).

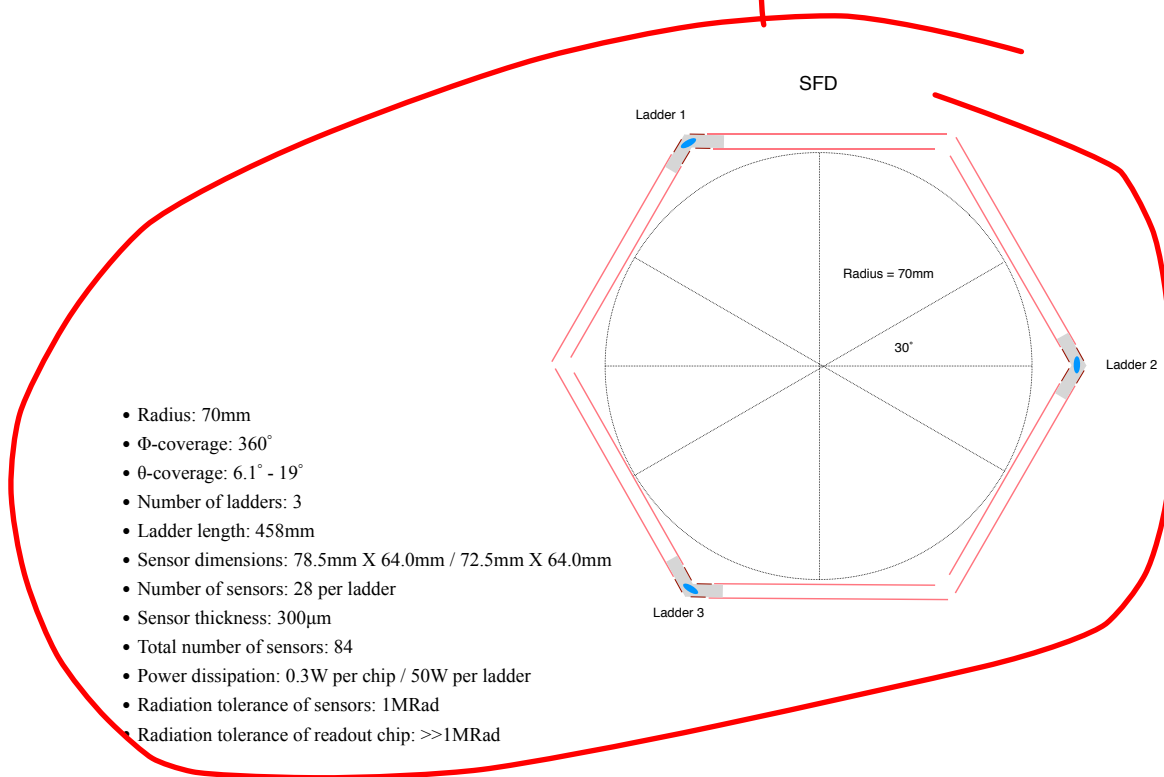


FIG. 33: Cross-section view of the DarkLight Silicon Forward Detector (SFD).

Both detector systems consist of three ladder arrangements each with a central rigid ceramic support frame. The support frame material has to be carefully chosen to provide proper rigidity and good thermal conductivity while at the same time minimizing outgassing. The support frame has an embedded cooling tube. Each support frame will support two silicon sensors on either side with a total of seven silicon sensors in a row as shown in Figures 34 and 35, respectively. Each sensor is only held in place on one side. The actual active area therefore consists of only two $300\mu\text{m}$ thick sensors providing a total radiation length of approximately $0.65\% X_0$. The inner most sensor and the front-end electronics part will be optimized for the recoil proton measurement while the outer sensor is focusing on the hit location measurement of the final-state leptons. The combination of both is meant to aid in distinguishing recoil protons from final-state leptons.

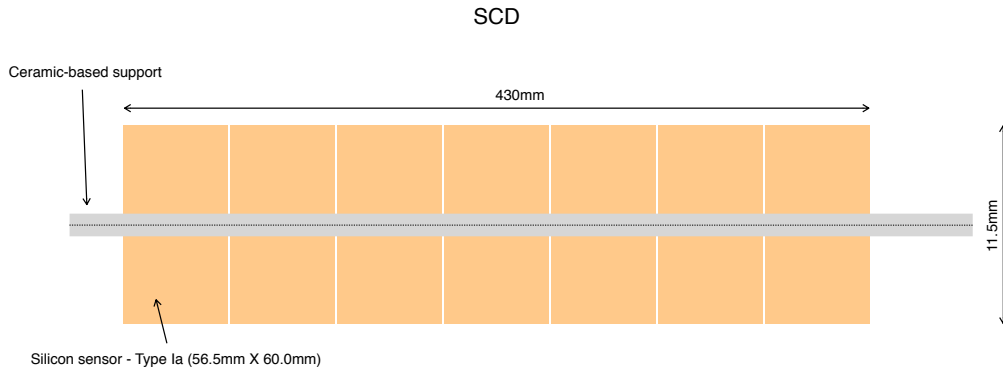


FIG. 34: Side view of the DarkLight Silicon Central Detector (SCD).



FIG. 35: Side view of the DarkLight Silicon Central Detector (SCD).

Silicon ladder concept and support structure

Figure 36 shows a cross-section of a ladder for the Silicon Central Detector (SCD) (left) and the Silicon Forward Detector (SFD) (right). Each sensor is glued on a central ceramic-based support frame in addition to the actual readout chip. Three ladder arrangements are needed for the SCD and SFD.

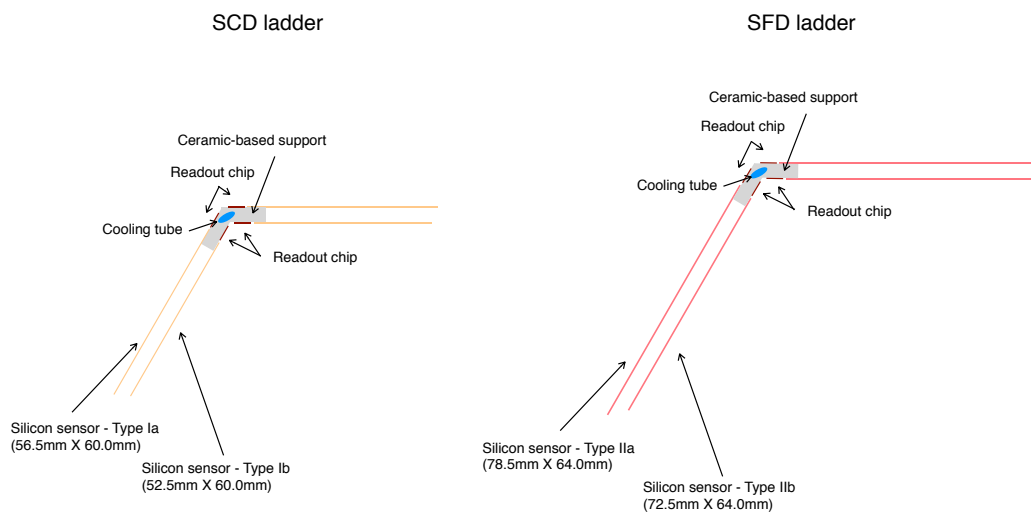


FIG. 36: Cross-section of the ladder.

Silicon sensors and readout system

As discussed earlier, the sensors are based on single-sided silicon sensors, specifically double-metal layer sensors. The manufacturing techniques for such silicon sensors are well

established. The preference is to produce single sided devices with p-implants on n-bulk silicon and poly-silicon biased. Those sensors are relatively easy to produce with high yields and can also be handled without much difficulty in a standard semi-conductor lab. In contrast, double-sided devices have lower yields (thus more expensive) and need special equipment to handle them. Several experiments such as PHOBOS [?] and STAR [?] have extensive experience in dealing with those type of sensors. The final choice of a readout chip has not been made yet as well as the actual layout of the readout hybrid. Figure 37 shows a cross-section of a double-metal silicon sensor. Those type of sensors are radiation hard sensors at the level of 1 Mrad.

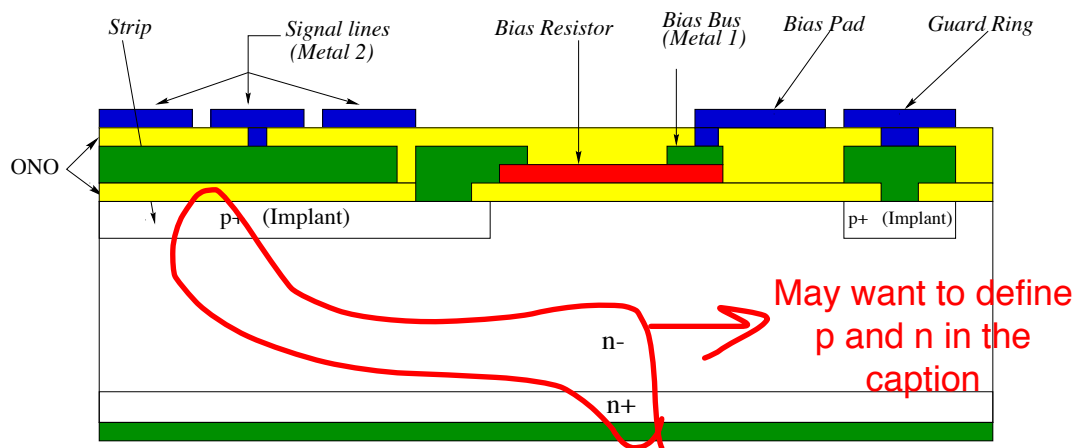
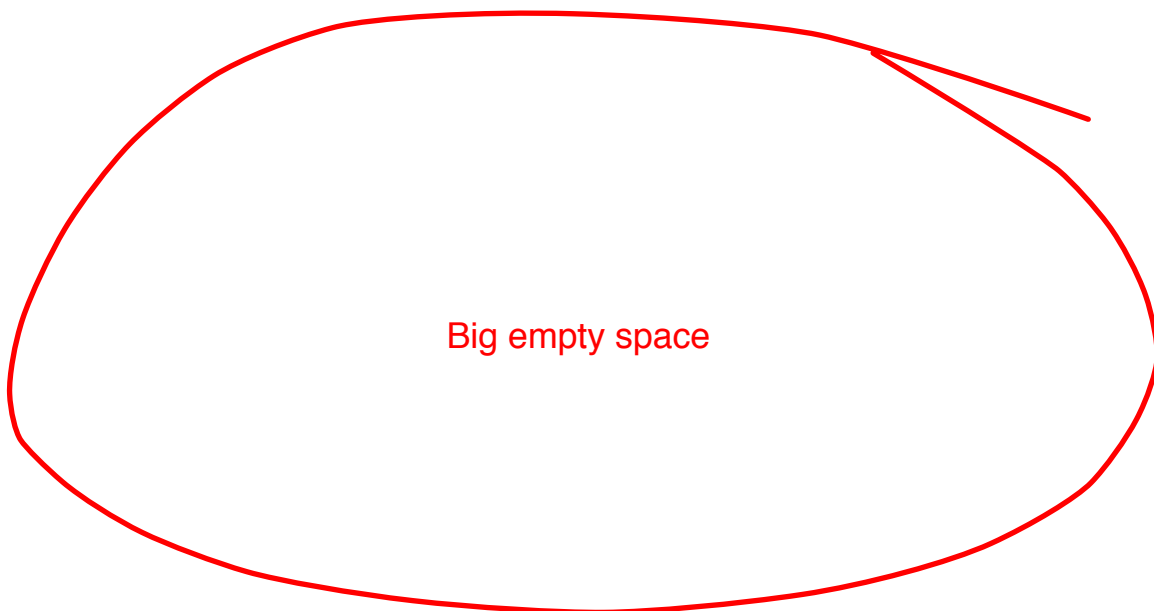


FIG. 37: Silicon pad sensor.



Cooling system

The expected heat dissipation for each silicon system is about 50W per ladder, 150W for the whole system of SCD and SFD each. A liquid cooling system is mandatory and would add at most 0.2% X_0 .

3. Scintillator detector

Really big blank
space

D. Target

1. Concept

The conceptual design of the target is shown in Fig. 38. The target gas is contained inside a beam pipe between two small-diameter ~~X~~ outflow channels centered on the beam axis upstream and downstream of the interaction region. The upstream outflow channel is embedded in a massive tungsten collimator designed to absorb any beam halo outside the channel diameter. The channel is recessed from the collimator exit to shield the detectors from electrons scattered form the channel entrance edge. The target gas parameters for a hydrogen target at room temperature are listed in Table IX. The gas pressure required to produce a target thickness of 10^{19} atoms/cm² in a 10 cm long interaction region results in viscous laminar gas flow through the outflow channels. The corresponding gas flow characteristics (Mach number η , Reynolds number R_e , pressure p , and target thickness t) at the entrance to the outflow channels of 2 mm diameter and 5 cm length are shown in Fig. 39 as functions of the outflow rate Q . These rates of tens of Torr-liter/s require sizable blower-type pumps at the first stages of the vacuum pumping cascades. To handle the required gas flow rates of tens of Torr-liter/s and reduce the gas pressure in the beam pipe to levels below 10^{-8} Torr required by the FEL, a set of three pumping stages is needed starting with a large mechanical booster pump followed by two turbo pump stages separated by flow limiters.

The innermost proton detectors inside the target gas volume are dimensioned to lie outside the envelope of Møller electrons emanating from the interaction region and contained by the magnetic field. The Møller envelope is shown in Fig. 38. Near the exit from this field, the Møller electrons are absorbed in a Møller dump made of graphite to minimize showering and shielded with lead. The pipe containing the gas and the proton detectors contains a section made of beryllium in the region of acceptance (25° to 165°) for electrons in order to minimize electron scattering.

In addition, we have considered the possible use of plasma windows [?] to provide a conductance limiter to generate the required target thickness. A plasma window's viscosity and high temperature allows the separation of gas at pressures ≈ 1 atmosphere from vacuum. It could allow larger diameter conductance tubes and reduce the gas flow. Fig. 40 shows a possible layout using 6 mm diameter plasma portholes. This option is under consideration.

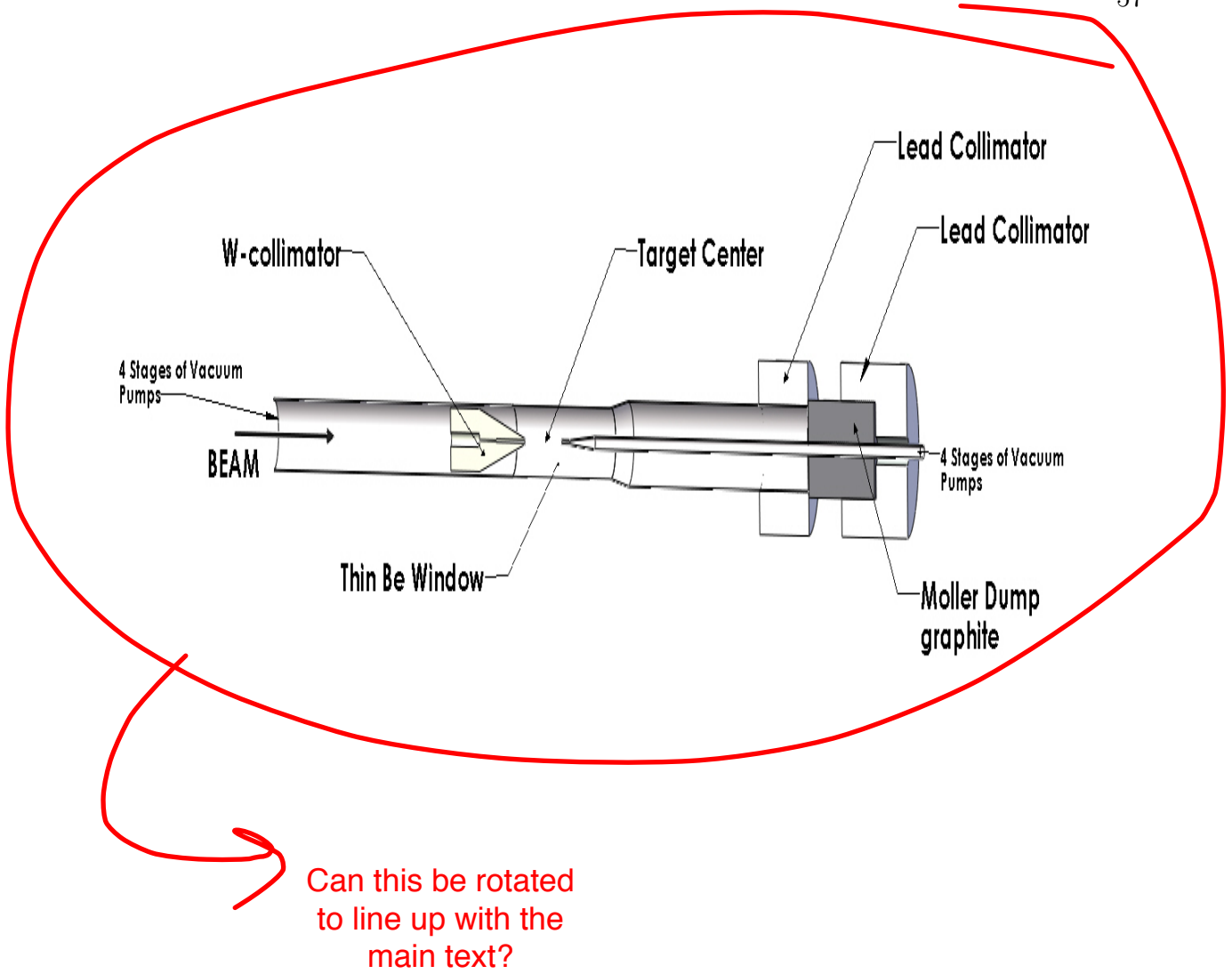


FIG. 38: Schematic layout of the proposed DarkLight windowless hydrogen gas target.

TABLE IX: Gas target specifications for the DarkLight experiment.

Outflow channel diameter	$D=2$ mm
Outflow channel length	$l= 5$ cm
Mach number at channel entrance	$\eta = 0.18$
Reynolds number at channel entrance	$R_e = 250$
Target pressure	$p = 12$ Torr
Target thickness	$t = 10^{19}$ atoms/cm ²
Gas outflow rate in each channel	$Q = 15$ Torr-liter/s

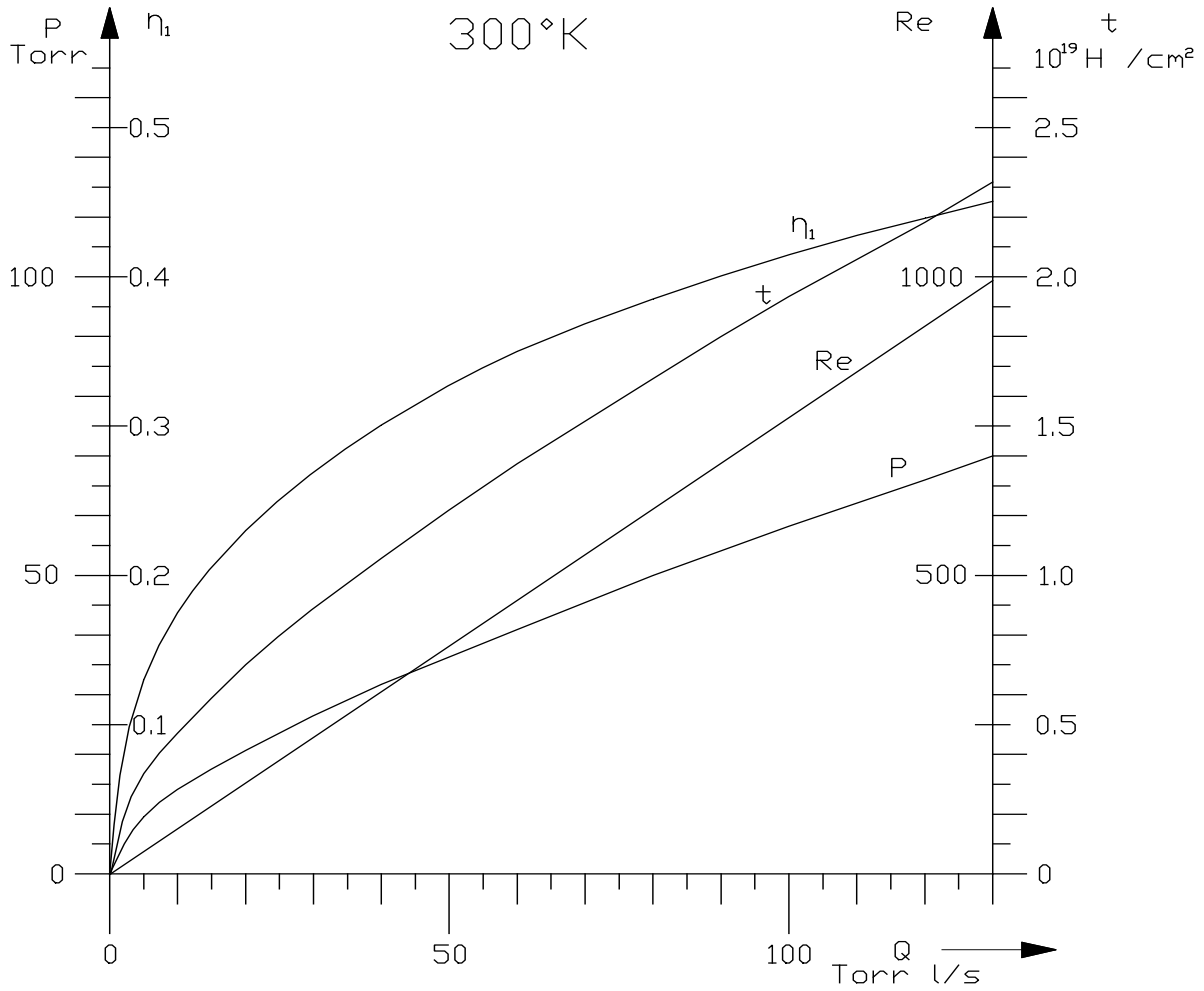


FIG. 39: Gas flow characteristics vs. outflow rate Q .

2. Beam interaction with the target

Calculations of the interaction of the 100 MeV electron beam and the gas target have been carried out for both hydrogen and xenon targets. While DarkLight is initially proposed

$$F(\tau) = 1 - \beta^2 + \frac{\frac{1}{8}\tau^2 - (2\tau + 1) \ln 2}{(\tau + 1)^2}$$

where τ is the kinetic energy of the electron in units of the electron mass. The electrons are energetic enough that the shell-correction is definitely negligible ($C = 0$). The mean excitation potentials are $I_H \approx 19$ eV and for Xenon is $I_{Xe} \approx 482$ eV.

From [?], we can estimate the density effect in hydrogen with:

$$\delta_H = 4.6X - 9.6 + 0.035(3.5 - X)^{6.79}$$

$$\delta_{Xe} = 4.6X - 12.7 + 0.133(5.0 - X)^{3.02}$$

← When $X = \log_{10}(\beta\gamma) = \log_{10}(200) \approx 2.30$, we get $\delta_H \approx 1.2$ and $\delta_{Xe} \approx 0.6$.

Putting this all together, we get that the energy loss due to ionization is

$$\Delta E_H/\sigma_H = (2.6 \times 10^{-25} \text{ MeV cm}^2)34.5 \approx 8.8 \times 10^{-24} \text{ MeV cm}^2$$

$$\Delta E_{Xe}/\sigma_{Xe} = (1.4 \times 10^{-23} \text{ MeV cm}^2)28.6 \approx 4 \times 10^{-22} \text{ MeV cm}^2$$

For a target of thickness 10^{19} hydrogen atoms cm^{-2} , these energy losses are negligible.

Bremsstrahlung

When $E_0 \gg 137m_e c^2 Z^{-1/3}$, we can use complete screening as an approximation. The total cross subsection is given by:

$$\frac{d\sigma}{d\omega} \approx 4 \frac{\alpha r_0^2}{\omega} Z(Z+1) \left[\left(1 - \frac{2}{3}\varepsilon + \varepsilon^2 \right) \ln \frac{183}{Z^{1/3}} + \frac{1}{9}\varepsilon \right]$$

← where

$$\varepsilon = \frac{E_0 - \hbar\omega}{E_0}$$

The energy loss is given by multiplying the cross subsection by the photon energy and integrating over all possible photon energies (approximately ε from 0 to 1):

$$- \left(\frac{dE}{dx} \right) = N \int_0^{E_0/\hbar} \hbar\omega \frac{d\sigma}{d\omega} d\omega = N E_0 \alpha r_0^2 Z(Z+1) \left(\frac{1}{18} + \ln 183 \right)$$

Thus, the energy loss over the cross-subsectional density is

$$\Delta E_{\text{H}}/\sigma_{\text{H}} \approx 4 \times 10^{-25} \text{ MeV cm}^2$$

$$\Delta E_{\text{Xe}}/\sigma_{\text{Xe}} \approx 7 \times 10^{-22} \text{ MeV cm}^2$$

Again, for the design target thickness of 10^{19} hydrogen atoms cm^{-2} , these energy losses are negligible.

Mott Scattering

Since the mass of the nucleus is large compared to the energy of the electron, we will neglect recoil of the proton and use the center-of-mass Mott cross subsection:

$$\frac{d\sigma}{d\Omega} = \left(\frac{Ze^2}{2E} \right)^2 \frac{\cos^2 \theta/2}{\sin^4 \theta/2}$$

Integrating over the solid angle:

$$\sigma = (6 \times 10^{-30} \text{ cm}^2) Z^2 \int_{\theta_c}^{\pi} \cot^3(\theta/2) d\theta \approx (2 \times 10^{-29} \text{ cm}^2) Z^2 \theta_c^{-2}$$

θ_c is the acceptance angle for the beam after interaction with the target. If we pick $\theta_c = 1$ mrad, for example, the cross subsection for hydrogen is $3 \times 10^{-23} \text{ cm}^2$ and for xenon is $9 \times 10^{-20} \text{ cm}^2$.

Møller Scattering

The scattering angle of the higher-energy electron is given by:

$$\cos^2 \theta = \frac{(E_0 + mc^2)(E_0 - E)}{(E_0 - mc^2)(E_0 - E + 2mc^2)}$$

and for the lower-energy electron:

$$\cos^2 \theta' = \frac{(E - mc^2)(E_0 + mc^2)}{(E_0 - mc^2)(E + mc^2)}$$

as determined by kinematics, where E is the final energy of the electron initially at rest.

The total cross subsection is

$$\sigma = 2\pi \frac{Z^2 e^4}{mc^2} \int_{E_c - mc^2}^{E_0/2} \frac{1}{E^2} dE$$

to first order. $\theta_c = 1$ mrad corresponds to an energy of $E_c - mc^2 = 0.01$ MeV. This corresponds to a cross subsection the same size as the Mott cross subsection for both hydrogen and xenon.



Big empty space

E. Integration

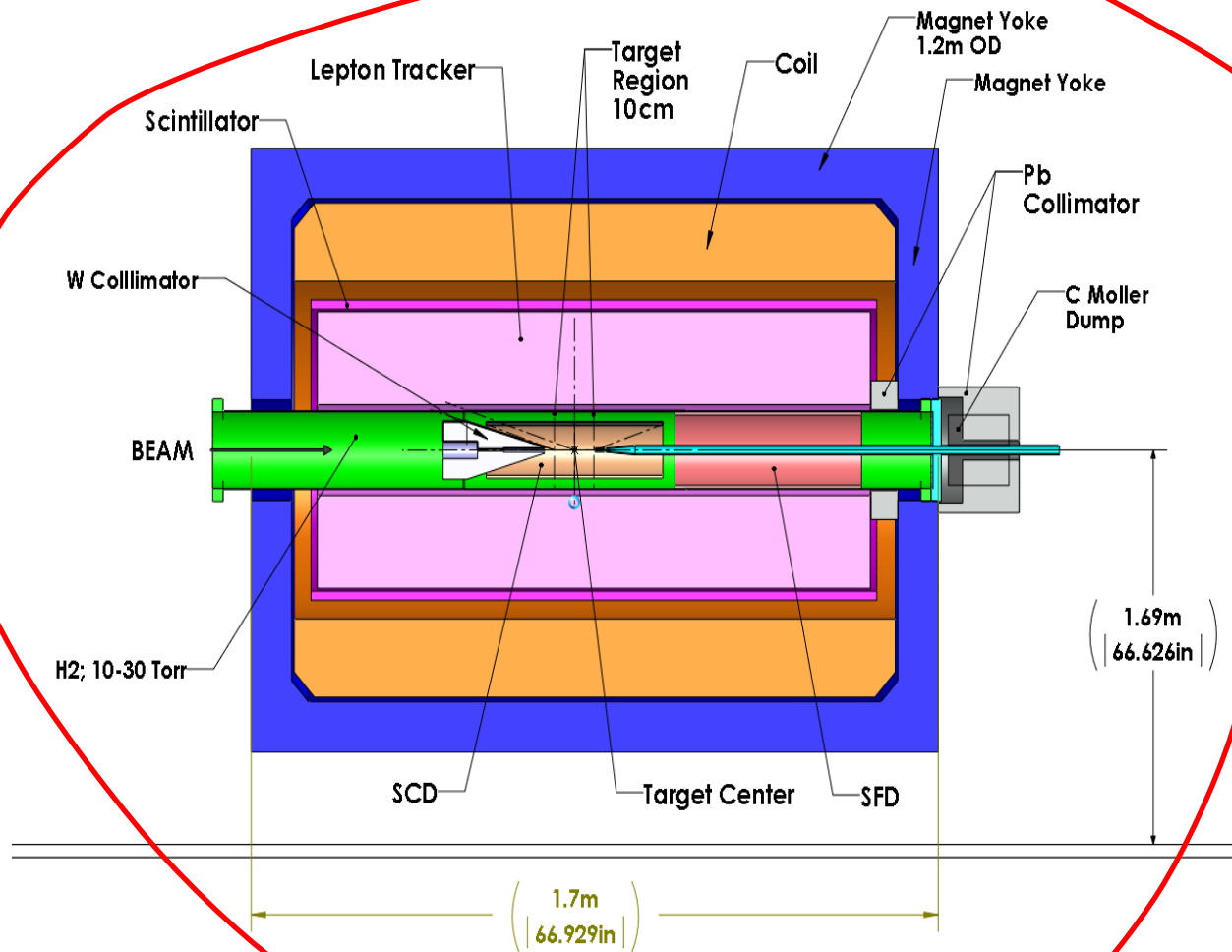
The Darklight detector occupies a small footprint while having a full array of detectors. See Figs. 41 and 42. This will present challenges in assembly as well as providing services to the detector. The limited space will drive many of the design features for the magnet and detectors.  Extra space

The fact that the magnet is a solenoid means that we cannot easily have a split magnet design. The magnet therefore will be of a barrel design. The detectors and vacuum system will have to be designed to be inserted from the ends of the magnet. We will design the magnet endcaps to be easily removable to accommodate this constraint and allow assembly of the detectors and vacuum system.

The lepton tracker and scintillator detector will have a cradle support. The proton detector and collimator will be located and supported inside the vacuum system. The vacuum system will then be instrumented with cabling and cooling services. This assembly will then be inserted into the lepton tracker and attached via kinematic mounts to the cradle support of the lepton tracker. This sub-assembly will then be inserted into the magnet bore via assembly fixturing. The cradle support will then be mounted to the magnet steel. In the design of the magnet and sub-systems we will have to be sensitive to providing adequate space for these supports and services.

The gas system will be remotely located. Due to the high flows the vacuum system will be substantial. However, most of the pumping will take place outside of the footprint of the Darklight detector so integration will be more important in regards to the inlet and outlet beamline.

The Darklight detector as a whole will be mounted on rails to allow retraction and insertion into the beamline. This assists us in assembly of the system. This will also allow us to perform limited repair in the event of equipment failures.



Same fig as an earlier one

FIG. 41: Schematic layout of the DarkLight experiment.

F. Trigger

The resonance signal of A' decay lies on top of a large QED background and both must be detected amidst even larger elastic scattering and Møller rates. These large rates require a trigger able to select events with a proton and three leptons in the final state. We propose a trigger concept as follows:

- The TPC tracker will be used as the primary trigger source. The estimated rate of the TPC is 20 MHz. The inner radius of the tracker is at 100 mm from the beam line to exclude the high rate Møllers.
- The current TPC prototype uses the AFTER readout chip.

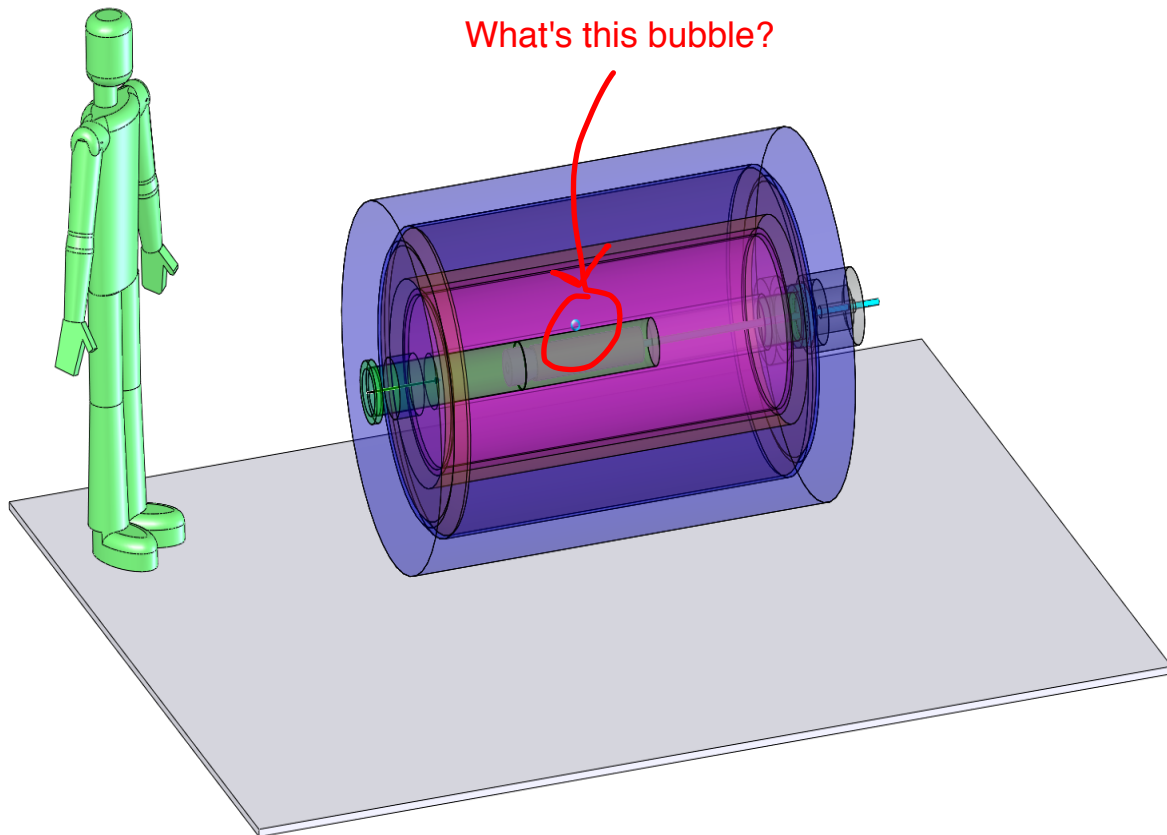


FIG. 42: The scale of the DarkLight experiment.

- Data from the readout chip is then digitized (if not already) and fed into the trigger pipeline. The pipeline will perform the following:
 - Hit detection
 - Zero suppression
 - Preliminary track construction
 - Track angle determination
 - Charge determination
 - Data-packaging to DAQ
- Triggers will be issued by the system based on the angle of the tracks and number of particles. One example is triggering on a lepton with $\theta > 90^\circ$ as well as having 3 lepton tracks. We estimate trigger rate here of 1MHz.
- The next level trigger uses inputs from the proton detector to further require that a

proton with energy > 0.5 MeV was detected.

- We estimate that this will result in a 10 kHz trigger rate which will be fed into the event builder and written to disk.
- We may also consider using the S-ALTRO chip developed by CERN. The S-ALTERO chip provides onboard ADC conversion, baseline correction, and zero suppression. This will reduce the data-rate in the next stage of the trigger, and reduce the processing power required. The SPADIC chip is another readout possibility.

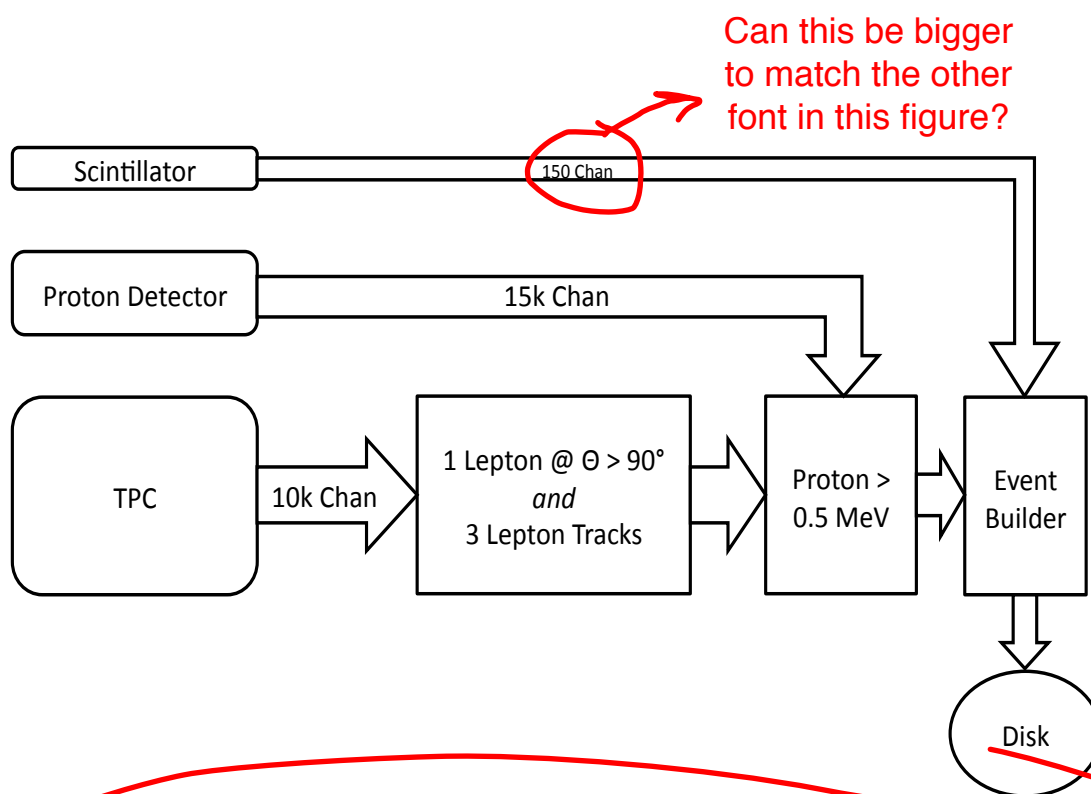


FIG. 43: Trigger block diagram for the DarkLight experiment.

We believe that such a hierarchical trigger scheme can provide the efficiency rates necessary for the experiment.

VI. EXPECTED PERFORMANCE

The DarkLight experiment offers unique ability to search for resonances in the 10-100 MeV range because of three important features:

- Full reconstruction of the four particle final state with reasonable Efficiency ~~efficiency~~
- Average invariant mass resolution of 1 MeV across the entire kinematic range
- Reasonable photon identification for A' decays to invisible final states

Reconstruction of all final state particles presents the major advantage and key challenge to the DarkLight experiment. The reconstruction of all final state particles will allow strong application of kinematic constraints, leading to high background rejection. A tracking system extending from 105 to 300 mm in cylindrical radius ρ and in the forward directions acts to identify the final state leptons and measure their momenta precisely.

Fig. 44 shows how the e^+e^- from the A' decay shares energy. Near the upper kinematic boundary of the A' mass of 92 MeV, the A' is nearly at rest and the leptons come out with similar energies around 40 MeV, while ~~a~~ ^{at} the lower end of the kinematic range, the energies of the leptons may be very different. We have carried out our planning based on optimizing the detector and run plan for all A' masses in the 10-100 MeV range. We will discuss possible modifications to this below.

This sentence needs to be reworded

The geometrical design and choice of field are driven by the kinematics of the Moller and elastic backgrounds. The 0.5 T field, necessary to confine the Moller electrons, and the 50 mm inner tracking radius make impose a $p_T > 10$ MeV cut on the final state leptons. The elastic rates in the forward region restrict the minimum forward tracking angle to $\theta_l, 25^\circ$ (there is no physics restriction on the backward scattering angle, but very few events lie in this region) and the elastic backgrounds restrict the minimum proton kinetic energy to $K_p < 1$ MeV. Combining these conditions gives an acceptance cross section as a function of A' mass shown in Fig. 45. For most of the cross section, the signal cross section lies in the range 0.01-10 pb and should be compared with a QED background cross section (across all A' masses) of about 10^5 pb.

Identification of the recoil proton also presents a key ingredient. Fig. ?? shows the ability of the silicon recoil detector to separate leptons from protons and the energy the proton energy measurement. Detection of the proton is not the dominant limitation on the

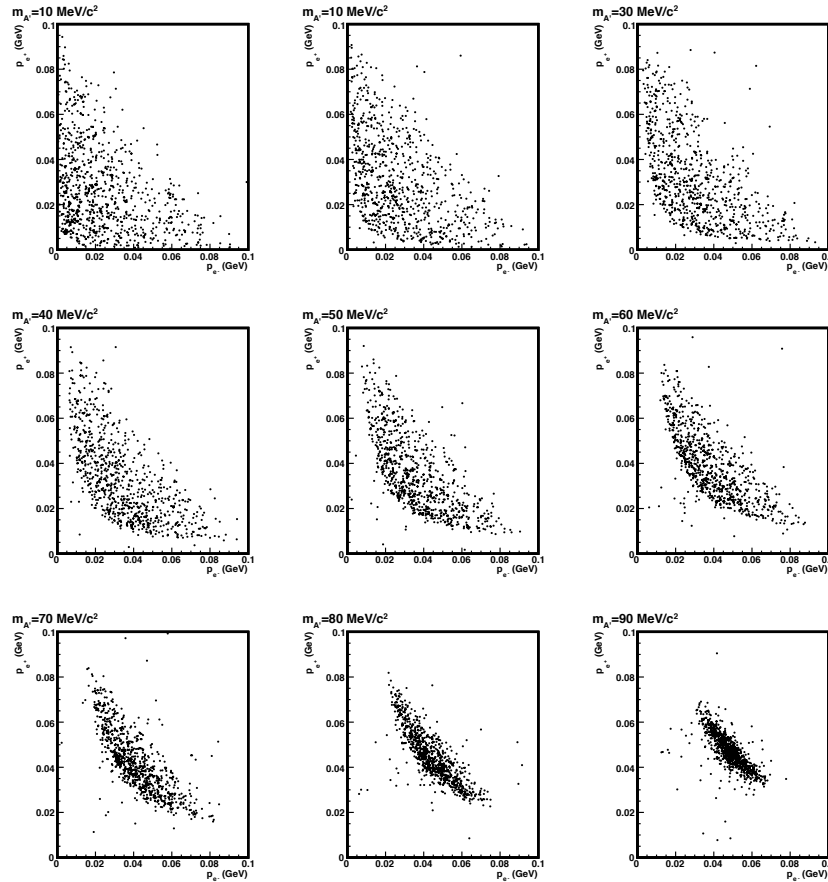


FIG. 44: Sharing of lepton momenta. Each scatter plot shows the reconstructed momenta of the e^+e^- pair from different A' masses.

efficiency. However, the 30% uncertainty on the proton energy measurement does dominate the total ~~uncertain~~ ^{uncertainty} on the measurement of the total energy and momentum of the event,

Fig. 47. \rightarrow as shown in Fig 47.

The second key feature of DarkLight is the e^+e^- mass resolution. The GEM-TPC has demonstrated a momentum resolution of $\sigma_{p_T}/p_T = 0.06$ at $p_T = 200$ MeV ~~over~~ over an angular range relevant for DarkLight and we have approximately verified this with our Monte Carlo. Along with the inner tracker wall, the proton detector and beam pipe in our current design total $0.01 X_0$, giving an invariant mass resolution ranging from 0.2-2 MeV over the 10-100 MeV range Fig. 48. \rightarrow as shown in Fig 48.

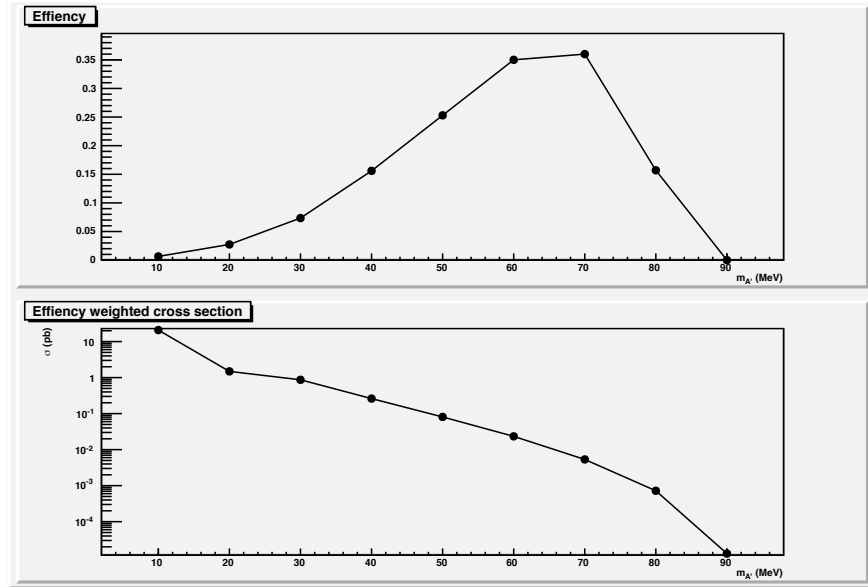


FIG. 45: Upper panel shows four particle final state detection efficiency. Lower panel shows efficiency weighted cross section for a $\alpha' = 10^8$. The lower efficiency at the low mass end results from loss of leptons with $p_T < 10$ MeV, as is apparent from Fig. 44. at

VII. RESOURCES AND SCHEDULE

↳ Missing section

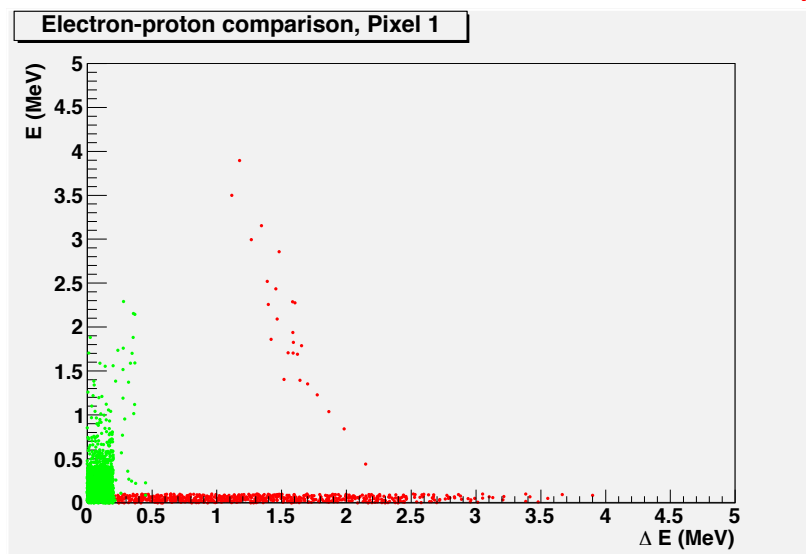
VIII. SUMMARY

↳ Is this true? An important aspect, absolutely, but the origin?

The DarkLight experiment provides a unique opportunity to search for the A' boson that could explain the origin of dark matter. DarkLight will be a challenging experiment, but an achievable one in the coming five years. Over the same time, results from cosmic ray and nuclear recoil experiments and the LHC may shape a new picture of dark matter, one in which DarkLight will play a key role.

This proposal has laid out a scientific case for DarkLight and shown the experiment is technically feasible at the Jefferson Lab Free Electron Laser. We are asking for an endorsement for DarkLight from PAC37 and PAC39 in order to move forward with the design of the experiment in the coming years. An endorsement of DarkLight will also enable us to begin discussions with Jefferson Lab and the agencies for support of the project.

Our formal beam-time request at the FEL request to carry out the measurement we have proposed is for the equivalent of 60 running days (assuming 100% efficiency) for data taking and the equivalent of 30 running days (assuming 100% efficiency) for beam studies,



Which is protons?
Which is electrons?

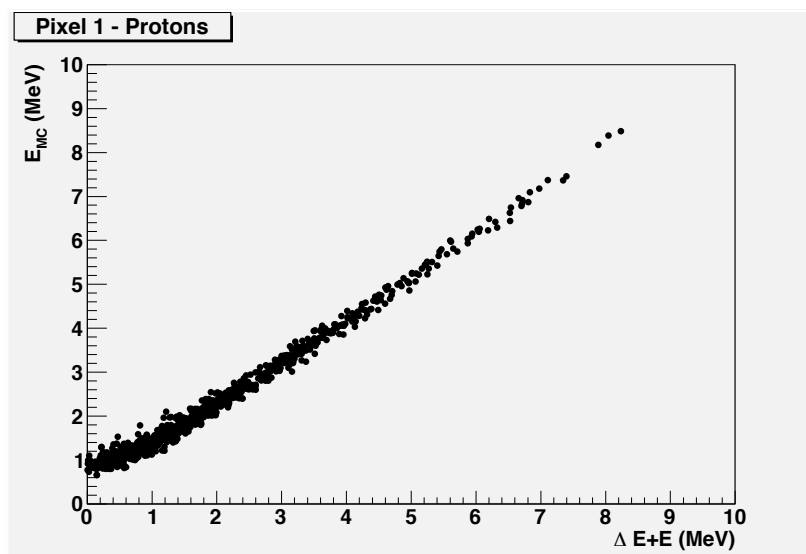


FIG. 46: Upper panel shows the separation between protons and electrons based on the total energy in a 1 mm^2 area on the proton detector. The lower panel shows the total proton energy reconstructed from the pixel detector compared with the initial energy from the Monte Carlo. The bend at low energies is from energy loss of the proton in the target region of the detector.

FIG. 47: Total reconstructed energy and momentum.

Where is the figure?

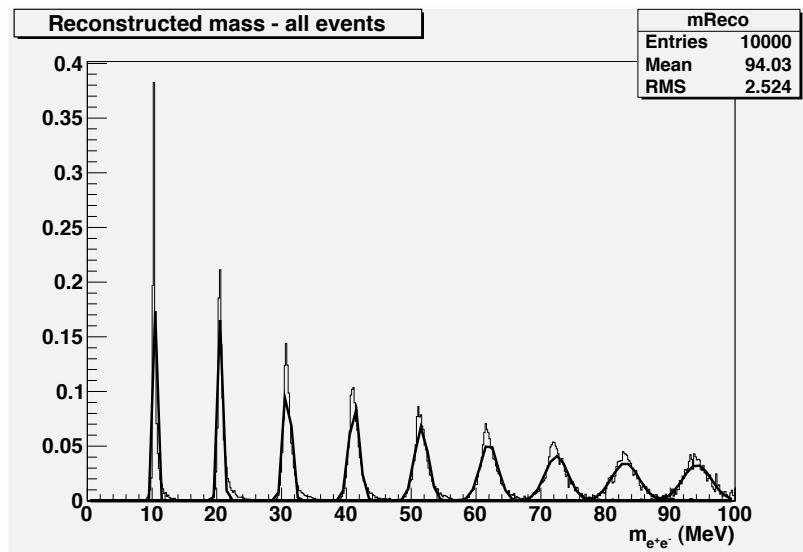


FIG. 48: Upper panel shows fits to reconstructed masses. Lower panel shows resolution.

check-out and calibration.

[1] In this context, the A' is often referred to as a U -boson.